Performance evaluation of four cascade impactors for airborne UFP collection: Influence of particle type, concentration, mass and chemical nature

Elisabeth Eckenberger[1], Andreas Mittereder[2], Nadine Gawlitta[3+4], Jürgen Schnelle-Kreis[3+4], Martin Sklorz[4], Dieter Brüggemann[2], Ralf Zimmermann[3+4], Anke C. Nölscher[1]

[1] Bayreuth Center of Ecology and Environmental Research (BayCEER), University of Bayreuth, Germany
[2] Department of Engineering Thermodynamics and Transport Processes, University of Bayreuth, Germany
[3] Comprehensive Molecular Analytics (CMA), Helmholtz Munich, Germany
[4] Chair of Analytical Chemistry, Institute of Chemistry, University of Rostock, Germany

Correspondence to: Elisabeth Eckenberger (Elisabeth.eckenberger@uni-bayreuth.de), Anke C. Nölscher (Anke.noelscher@uni-bayreuth.de)

Abstract. Ultrafine particles (UFP) have aerodynamic diameters of 100 nm or less. As UFP potentially impact human and environmental health, their chemical composition is of interest. However, their small mass challenges sampling and chemical characterization methods. Therefore, we conducted a comprehensive characterization and comparison of four cascade impactors suitable to separate and collect UFP, namely 120R MOUDI (Micro-Orifice Uniform Deposit Impactor), ultraMOUDI, ELPI (Electrical Low-Pressure Impactor), and PENS (Personal Nanoparticle Sampler), under controlled laboratory conditions and in a field application.

In the laboratory, we evaluated pressure drop, cut-off diameters, steepness of the cut-off curve, losses, particle bounce, and transmitted particle mass. We observed that the performance of the impactors varied between 59 and 116 nm in cut-off diameter (electromobility diameter). This was depending on the impactor's design and the type of test aerosol mixture, which was either salt particles (NaCl), simulated secondary organic aerosol (SimSOA), or soot. All impactors separated UFP, with the best agreement in cut-off diameters for SimSOA, showing maximum deviations of about 4 nm. The cut-off curve was steeper for soot compared to SimSOA and NaCl. Pressure drops were measured at 260±1 hPa (PENS), 420±2 hPa (ultraMOUDI), 600±3 hPa (120R MOUDI), and 690±3 hPa (ELPI). Losses were assessed as maximum transmission in the ultrafine fraction at 30 nm, resulting in 83±8% for PENS, 77±8% for ultraMOUDI, 75±8% for 120R MOUDI, and 69±7% for ELPI. We compared two additional impactor-specific factors crucial for mass-based analysis of organic marker compounds: evaporation of semi-volatile compounds due to high pressure drop across the impactor and material addition from larger particles bouncing off upper stages. Bounce-off was influenced by particle number concentration in the sampled air and could be partially mitigated by applying a coating to the upper impaction plates.

In the field application, we deployed the four cascade impactors side-by-side under environmental conditions to sample urban air. We analyzed six markers representing typical UFP sources and various molecular properties using HPLC-MS/FLD (high-performance liquid chromatography with mass spectrometry and fluorescence detection), namely benzo[a]pyrene (BaP), benzo[b]fluoranthene (BbF), levoglucosan (Levo), pinic acid (PA), terpenylic acid (TA), and N-(1,3-dimethylbutyl)-N'-phenyl-p-phenylenediamine (6PPD). The impactors showed the best agreement for the BaP and BbF. BaP had an average mass concentration of 175 ± 25 pg/m³ across all impactors and sampling days, but concentrations were about 29% higher when sampled with PENS or 30% lower when sampled with 120R MOUDI, indicating a maximum disagreement of nearly 60%.

The mass concentrations of the semi-volatile markers, PA, TA and Levo, were decreasing on average from PENS, to ultraMOUDI, to 120R and ELPI. We attributed this tendency to two effects: (1) Likely evaporation losses of those markers were driven by the pressure drop within the impactor, which was indeed increasing from PENS to ELPI. (2) Despite the applied coating, bounce-off might have affected the smallest impactors (PENS and ultraMOUDI) the most as these have less stages for retaining larger particles and fragments.

1 Introduction

The characterization of ultrafine particles (UFP) in the atmosphere can be a key for understanding the cause and impact of air pollution. UFP are defined as particulate matter with aerodynamic diameters of 100 nanometers and less. They have gained considerable attention due to their potential impacts on human health and the environment (Kumar et al., 2014, 2021; Schwarz et al., 2023). Furthermore, airborne UFP are naturally linked to weather and climate, as they might alter the radiative budget of Earth directly, or indirectly when growing and activating to form cloud droplets (Junkermann et al., 2022). The size and the chemical composition of UFP, thus, are crucial properties for assessing their sources, atmospheric fate, and potential adverse effects.

Information about size and chemical composition of airborne particulate matter can be collected via impactors. Impactors allow separating particles in an air sample based on their aerodynamic diameter (d_a). The physical separation of particles within an impactor is based on the particle's inertia, which causes relatively smaller particles to continue moving when the airflow bends sharply, e.g. when forced through nozzles, orifices, or slits (Baron and Willeke, 2011). Upon separation, the particles can be collected on the impaction plates or downstream of the impactor, when placing filter substrates, such as aluminium foils, PTFE, or quartz fibre filters. Particles caught in the substrate can be extracted and undergo chemical analysis to determine their composition (Bein and Wexler, 2014; Canepari et al., 2010; Daher et al., 2011). To describe the separation and collection efficiency, the dp50, a value at which particles will be collected with 50% efficiency is used. The dp50, or cut-off diameter, for a given impactor design will depend on the nozzle diameters and the flow rate.

A stack of impactors, impaction and nozzle plate pairs, is a cascade impactor. Within the cascade impactor, the nozzles or slits become increasingly smaller, so that the air moves increasingly faster through these orifices. Large particles impact early, while smaller particles travel further through the impactor and are collected at later stages. Cascade impactors were first employed in the 1860ies to study the relationship of airborne particles and diseases (Marple, 2004). Later models enabled size classification in a sub-µm range (May, 1945; Berner et al., 1979; Brink, 1958; Mitchell and Pilcher, 1959). Examples are the Berner and Anderson impactors (Hata et al., 2012; Hillamo and Kauppinen, 1991), the electrical low-pressure impactor (ELPI), which can be used for real-time size distribution measurements (Keskinen et al., 1992; Marjamäki et al., 2000, Held et al., 2008), the micro-orifice uniform deposit impactor (MOUDI), which is capable of capturing particles as small as 0.056 µm (Marple et al., 1991), miniaturized impactors, such as the Personal Nanoparticle Sampler (PENS) (Tsai et al., 2012), and novel developments of small samplers for ultrafine particles (Thongyen et al., 2015, Kumsanlas et al., 2019, Gong et al., 2023).

Several recent studies focussed on airborne UFP chemical analysis upon cascade impactor sampling. For example, the MOUDI has been applied at Frankfurt Airport to analyze size-resolved UFP emissions from aircrafts, identifying organic compounds such as esters from jet engine oils (Ungeheuer et al., 2021). In Rio de Janeiro the MOUDI was used to collect ultrafine and coarser particles from vehicular emissions in an urban area and the trace element composition was analyzed across various

particle sizes, detecting cadmium, nickel, lead, chromium, and iron particularly in the UFP ranges (de Souza et al., 2021). The ELPI can be used for simultaneous real-time sampling of particle size distributions and offline chemical analysis, as e.g. done by Kim et al. in 2013, who classified and characterized airborne particulate matter in a rubber manufacturing plant. In the surroundings of a former electronic waste recycling facility, the ELPI was used to detect real-time airborne particles in the size range of 0.03–10 µm (Guo et al., 2023). Moreover, size-resolved chemical characterization of airborne particles from indoor sources, such as candles, mosquito-coils and cooking activities, highlighted heavy metals and polycyclic aromatic hydrocarbons (PAHs) in the ultrafine fraction (Caracci et al., 2024).. Similarly, other working environments were characterized in terms of personal exposure via the application of the portable PENS (e.g. (Pomata et al., 2023; Young et al., 2013). The PENS has also been employed for air quality studies such as in wintertime rural and urban China for the chemical analysis of biomass burning tracers such as Levoglucosan (Zhu et al., 2017). While not exhaustive, these examples underscore a growing number of applications and interest in diverse types of target analytes. This raises the question of comparability between cascade impactor applications for atmospheric ultrafine particle chemical analysis.

The challenge, particularly when it comes to the separation and collection of UFP from the atmosphere using cascade impactors, is unequivocally associated with the remarkably low mass of UFP. This low mass, as opposed to fine particulate matter (PM$_{2.5}$), presents a substantial hurdle in conducting gravimetric or chemical analysis. Specifically, UFP collection with cascade impactors is sensitive to the following aspects:

      (1) The **cut-off diameter** for UFP (dp50=100nm, referring to aerodynamic diameter) of the last impactor stage depends on its design and operational characteristics such as the diameter, nozzle size, flow rate, distances between plates, and its shape. Moreover, real atmospheric particles, of various shapes and densities, will vary in impaction behaviour and thus potentially influence the separation.

      (2) The **loss** of UFP on walls or earlier stages could retain particulate material.

      (3) During collection either larger particles bounce or break into fragments and re-entrain adding mass to the filter substrate dedicated for UFP or target UFP bounce-off from the collection substrate and are lost for analysis.

      (4) Semi-volatile particle-bound components may **evaporate** from already collected particulate surfaces during the ongoing sampling due to a reduced pressure within the impactor and continuous ventilation. This can result in alterations of the chemical composition due to interactions with the gaseous phase.

Therefore, in this study, we explored the cut-off diameter, potential losses, artefacts due to bounce-off and evaporation for four different cascade impactors, which are capable of separating and sampling UFP. Our overall aim was to identify and quantify organic marker compounds in the collected UFP. The four cascade impactors differed in design, flow rate, number of stages, among other factors. We expected, that these differences would significantly impact the abovementioned aspects and therefore lead to different results of analyzed mass concentrations of the selected organic marker compounds within the collected UFP.

2. Methods

2.1 Impactors for UFP Sampling

Today, several cascade impactors exist, which are either commercially available or newly developed (Crazzolara and Held, 2024; Ngagine et al., 2022; Järvinen et al., 2014; Romay and García-Ruiz, 2023; Marple et al., 2014; Tsai et al., 2012). For our comparison, we selected four commercially available models for sampling atmospheric UFP that cover different designs, flow rates, and stage numbers. Additionally, we wanted to sample all ≤100 nm particles on one substrate without further separation. Moreover, we envisioned the use of an automated filter changer in future applications which would be possible with all selected models. Some of these selected impactors required minor adjustments to make them suitable for achieving the final cut-off diameter at 100 nm. Apart from these adjustments, which are outlined in the following, the cascade impactors were operated as described by the manufacturers.

For each impactor and for each measurement, the aerosol flow was regulated between the impactor and its pump. The flow rate was determined at the impactors inlet with a Gilibrator 2 bubble flow meter and re-checked following each collection interval.

Rotating 10-stage 120R MOUDI-II: The MOUDI utilizes numerous micro-orifice nozzles to reduce jet velocity, pressure drop, particle bounce, and re-entrainment, while enhancing collection efficiency and enabling a uniform deposition on the impaction plate (Marple et al., 1991). Each pair of nozzle and impaction plate is called a stage. The uniform-deposit prevents particle build-up and allows a greater collection mass without overloading. It is further supported by rotating the impaction plates relative to the nozzles while distributing the sampled particles over the sampling substrates. Earlier models (MOUDI 110 and 115) achieve relative rotation between impaction and nozzle plates by rotating alternate impactor stages using external gears and hooks that mesh with an external drive shaft powered by an electric gear motor. In contrast, the newest model (120R MOUDI-II, MSP Corp., Shoreview, MN, USA), has impaction plates that are directly mounted onto miniature stepper motors, which are housed within a chamber situated in the center of each stage. Therefore, the 120R MOUDI-II offers an undisturbed flow path from the impaction plate to the next stage's nozzle plate. This design is expected to show relatively lower particle losses compared to previous models (Marple et al., 2014).

In this study, we modified the 120R MOUDI by removing the 0.56 nm stage (including the nozzle and impaction plates) located below the 100 nm cut-off diameter stage. This modification allowed us to collect all particles ≤100 nm in the original after-filter holder mounted at the impactor outlet. As recommended, we operated the 120R MOUDI-II at a flow rate of 30 L/min. It separated airborne particulate matter into nine fractions having nominal cut-off diameters (dp50) of 0.10, 0.18, 0.32, 0.56, 1.0, 1.8, 3.2, 5.6 and 10 μm. We equipped all upper stages with aluminium foils with a 47 mm diameter, that were greased

in a later stage of the experiments. We placed a 47 mm quartz fiber filter (QFF, Whatman QM-H) in the after-filter holder for collection of UFP.

Non-rotating 3-stage MOUDI (ultraMOUDI): In contrast to the 10-stage 120R MOUDI-II, this compact MOUDI model has three non-rotating stages (MOUDI 100-2.5-1-0.1. MSP Corp., Shoreview, MN, USA). The internal construction of these stages is similar to that of the models 110 and 115, while sharing the same inlet and outlet design. We asked the manufacturer for three stages with cut-off diameters at 0.1, 1 and 2.5 µm. Here, we employed the ultraMOUDI with aluminium foils (47 mm diameter) on the impaction plates. The after-filter holder was equipped with a 47 mm quartz fiber filter (Whatman QM-H). The flow rate through the impactor was 30 L/min. Due to its reduced size and weight, this impactor could be integrated in an automated sampler for independent long-term observations of UFP.

ELPI: The ELPI (Dekati Ltd. in Tampere, Finland, (Keskinen et al., 1992) separates and counts particles simultaneously on the respective stages while sampling. This way, the ELPI determines particle size distributions ranging from 30 nm to 10 µm. Sampled particles are first charged to a predetermined level. These charged particles are then classified by aerodynamic diameter within the cascade impactor. Lastly, a multichannel electrometer simultaneously measures the charges carried by the collected particles to each stage, providing a measurement for the particle number concentration. The particle classification is achieved using a multi-jet impactor, where stage 1 has the smallest and stage 13 has the largest cut-off diameter (0.03, 0.06, 0.09, 0.17, 0.26, 0.40, 0.65, 1.0, 1.6, 2.5. 4.4, 6.8, and 10 µm). The jet orifices are symmetrically drilled in rings around the center of each stage. Stage 1 of the impactor serves as a critical orifice, regulating the flow rate to 30 L/min and creating a low-pressure, which is thought to ensure the impaction of even the smallest particles (Marjamäki et al., 2000).

For this study, we extracted the cascade impactor component from the ELPI and considered it as a standalone impactor without the charger and electrometer. For the collection of UFP, we removed the stages with cut-off diameters of 0.03 and 0.06 µm to achieve a final cut-off size of 0.09 µm at stage 3. To maintain the flow characteristics, secure the impaction plates in the built-in tensioner, and ensure appropriate spacing between the nozzle and collection plates, placeholders were inserted instead. The flow was adjusted with a valve. On upper stages, aluminium foil filters (25mm, Dekati) were installed. For collection of UFP, a 37 mm QFF was installed in the after-filter holder provided by the manufacturer.

PENS: The PENS (Haze Control System Inc., Taiwan) was recently designed by Tsai et al. (2012) as a three-part system for the collection of airborne particles. The first part is a respirable cyclone that separates particles larger than 4 µm in aerodynamic diameter. The second part is a micro-orifice impactor, where particles with sizes from 0.1 to 4 µm impact on an impaction plate. The final part consists of a filter holder containing a 37 mm quartz fiber filter, which collects UFP. Compared to the previously described devices, the PENS is compact with dimensions of 107 mm in length and 44 mm in width, and a total weight of 240 g. This makes the PENS portable and useful for personal exposure studies (Young et al., 2013). The manufacturer

200   modified the PENS for this study to separate the particles in the fractions 2.5 and 0.1 µm and to operate at a sampling flow rate of 4 L/min. The impaction plate itself is not suitable to install a filter. For collecting of UFP within the afterfilter, we utilized a 37 mm quartz fiber filter (Whatman QM-H).

2.2 Overview of laboratory tests for evaluating the performance of the four impactors for UFP separation and collection

205   For testing the four cascade impactors under controlled conditions, we conducted a series of laboratory tests. Our objective was to determine the pressure-drop, transmission, UFP cut-off diameter, and potential artefacts of each impactor. Therefore, we generated three types of test aerosol and used reference instrumentation to quantify UFP. This way we detected the particle number size distribution before and after passing the test aerosol through the impactors.

2.2.1 Detection of particle number size distributions

210   We monitored the particle number size distribution for the four cascade impactors with two complementing instruments. For accurate and sensitive observations, a mobility particle size spectrometer (MPSS) was deployed. However, the analysis of cut-off performance for impactors with a pressure drop of several hundred hectopascal (hPa) posed a challenge to the MPSS flow regulation. Thus, for fast and repetitive measurements in low pressure, a real-time differential mobility particle spectrometer (DMS) was used. Yet, this instrument has comparatively low sensitivity.

215

MPSS

The MPSS (TROPOS) classifies and quantifies airborne particles based on the principle of the mobility of charged particles in an electric field (Wiedensohler et al., 2012, 2018). Sampled particles are neutralized to achieve a Fuchs equilibrium charge distribution, then classified by a Differential Mobility Analyzer (DMA) based on electrical mobility. The particle number size

220   distribution is obtained by scanning the voltage applied to the DMA, typically covering a range of 10 to 800 nm. The MPSS is capable of detecting down to 10 particles per cm³ per scan (Wiedensohler et al., 2012). The MPSS data were processed following the protocol by Wiedensohler et al. (2012), including corrections for particle losses and CPC counting efficiency. The MPSS measurements had an uncertainty of ±10%.

225   **DMS500**

The DMS500 (Cambustion) uses a corona diffusion charger and a classification column with electrometers to detect particle concentrations across a size range of 5 nm to 2.5 µm with a time-resolution of milliseconds (Symonds et al., 2007). The air sample is diluted twice before classification, leading to a comparatively low sensitivity of 170 cm⁻³ for 80 nm particles. The DMS500 was calibrated using polystyrene latex spheres (3320A/3495A, Thermo Scientific, NIST), and data were processed

230   using DMS software (DMS 6.09 complemented by DMW Excel Utilities 7.49). The overall uncertainty of the instrument was

±23%, calculated based on the relative standard deviation for the test particle mixtures mixtures (Cambustion Ltd., 2019, Symonds et al. (2004) (see 2.2.2).

2.2.2 Testparticle generation

235 To determine the cut-off characteristics of the individual impactors under controlled conditions, we used a laboratory test-bed consisting of a defined particle source, the test impactor, and the reference instrument to determine particle number size distributions, such as the MPSS or DMS500. If needed, the impactors were modified to have a cut-off diameter at 100 nm of the last stage (see 2.1.). Furthermore, we removed the after-filter holder in order to directly assess the transmitted particles with the online reference instruments. Instead, after the impactor a y-piece made of stainless steel (inner diameter 15 mm) was

240 installed directing the air flow to the detector and a pump. The pump was adjusted to achieve the correct overall sampling flow of the impactor. The test impactor was then connected to one of three different particle sources. The set-up is presented in Figure 1.
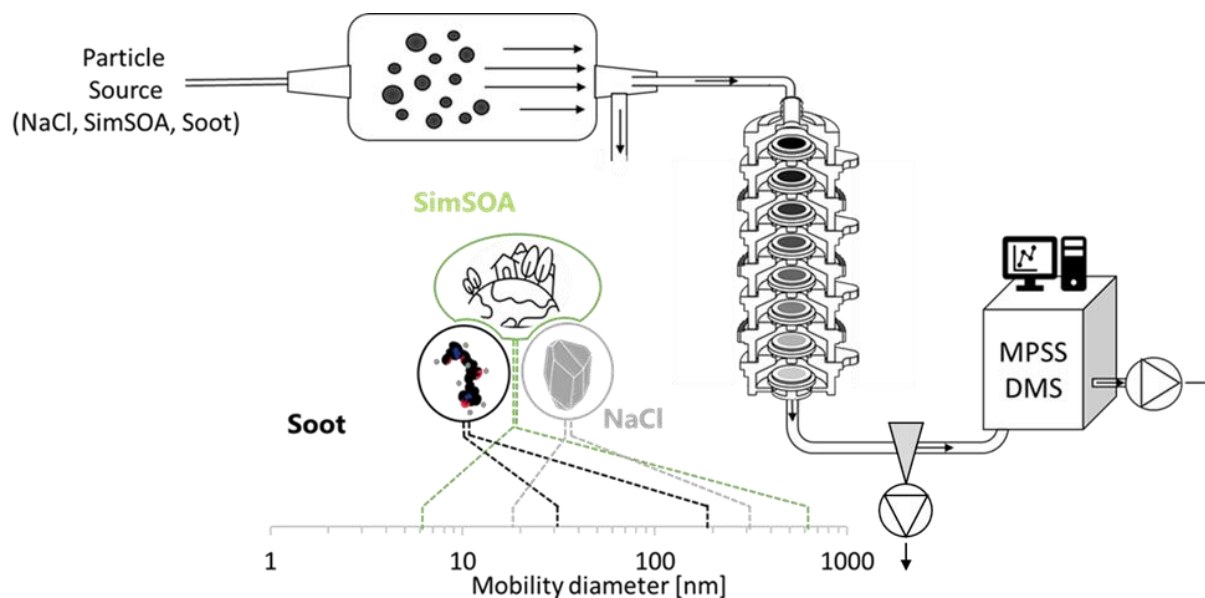
245 **Figure 1: Schematic experimental setup used to evaluate the cut-off characteristics of various impactors, namely 120R MOUDI, ELPI, PENS, and ultraMOUDI. Three different types of particles were generated: (1) NaCl (produced by spraying a saline solution), (2) SimSOA (generated through a chamber experiment involving particle formation from alpha-pinene and ozone, including seed particles), and (3) soot (produced by a diesel engine) (Section 2.2.2).**

250 NaCl particles

First, we generated salt particles from sodium chloride (NaCl). The particles were generated via a commercially available nebulizer (PARI, LC SPRINT, Type 023). The nebulizer was filled with a saturated solution of NaCl in millipore water. We

8

connected synthetic compressed air from the house line to the nebulizer and regulated it with a needle valve to 4 L/min. This aerosol flow was directed into a 30.5 L quartz glass flow tube for diluting, mixing, aging and drying. Since the majority of the impactors have a flow rate of 30 L/min, a dilution of 40 L/min synthetic air was also fed into the flow tube. At the flow tube outlet, the test impactor was connected in line with the reference instrument and the pump. This set-up allowed us to run tests for a time period of about 6-8 hours with a stable and relatively broad test particle number size distribution (Fig. 2).

With an estimate of density (ρ_p=2.16 g/cm³) and shape (χ=1) of the NaCl particles, we converted the electrical mobility diameter (d_m) given by the reference instruments to aerodynamic diameter (d_a) (Baron and Willeke, 2011). The aerodynamic diameter is the basis for the size-based separation of particles in the impactors and thus the critical value for evaluation and comparison.

Soot particles

Secondly, we tested the four impactors with diesel exhaust particles containing soot following the experimental setup as previously described by Mühlbauer et al. (2016). For our investigation, we employed a contemporary four-cylinder diesel engine supplied by Daimler AG (Model OM 651, Mercedes Benz, Germany). This engine is equipped with a common-rail system and features direct-acting piezoelectric injectors from Delphi Automotive PLC (United Kingdom). This production engine, equipped with a particle filter, complies with the European exhaust emission standard Euro 5. The engine was run with a speed of 1200 rounds per minute (rpm), an injection pressure of 700 bar, a throttle position maintained at 15%, and an exhaust gas recirculation (AGR) rate of 45%. The engine emissions were directly channelled from the exhaust pipe to the impactor to achieve a stable particle number size distribution around the 100 nm diameter range (Fig. 2).

SimSOA

Thirdly, we tested the impactors' performances with atmospheric simulated secondary organic aerosol (SimSOA). In order to conduct our tests at a stable mixture for several hours, we used one of the Bayreuth ATmospheric simulation CHambers (BATCH) (Ofner et al., 2011). Before each measurement, the 700 L cylindrical glass chamber was flushed with outdoor-air to introduce real environmental particles and trace gases. Subsequently, 0.05 mL of alpha-pinene was injected into the air flow, while a nebulizer delivered seed particles (saturated ammonium sulfate solution) into the chamber at a flow rate of 3 LPM for 3 minutes. After an additional 5 minutes, the pump supplying outdoor-air was switched off, and the solar simulator (UV Osram HMI, 4000 W, filtered with water-cooled glass plate, (Ofner et al., 2011; Zhao et al., 2008) was turned on for 15 minutes to stimulate ozone production and the subsequent formation of SimSOA. Prior to commencing the impactor measurements, the reference instruments were directly connected to the chamber to ensure suitable particle concentration and number size distribution (Fig. 2).
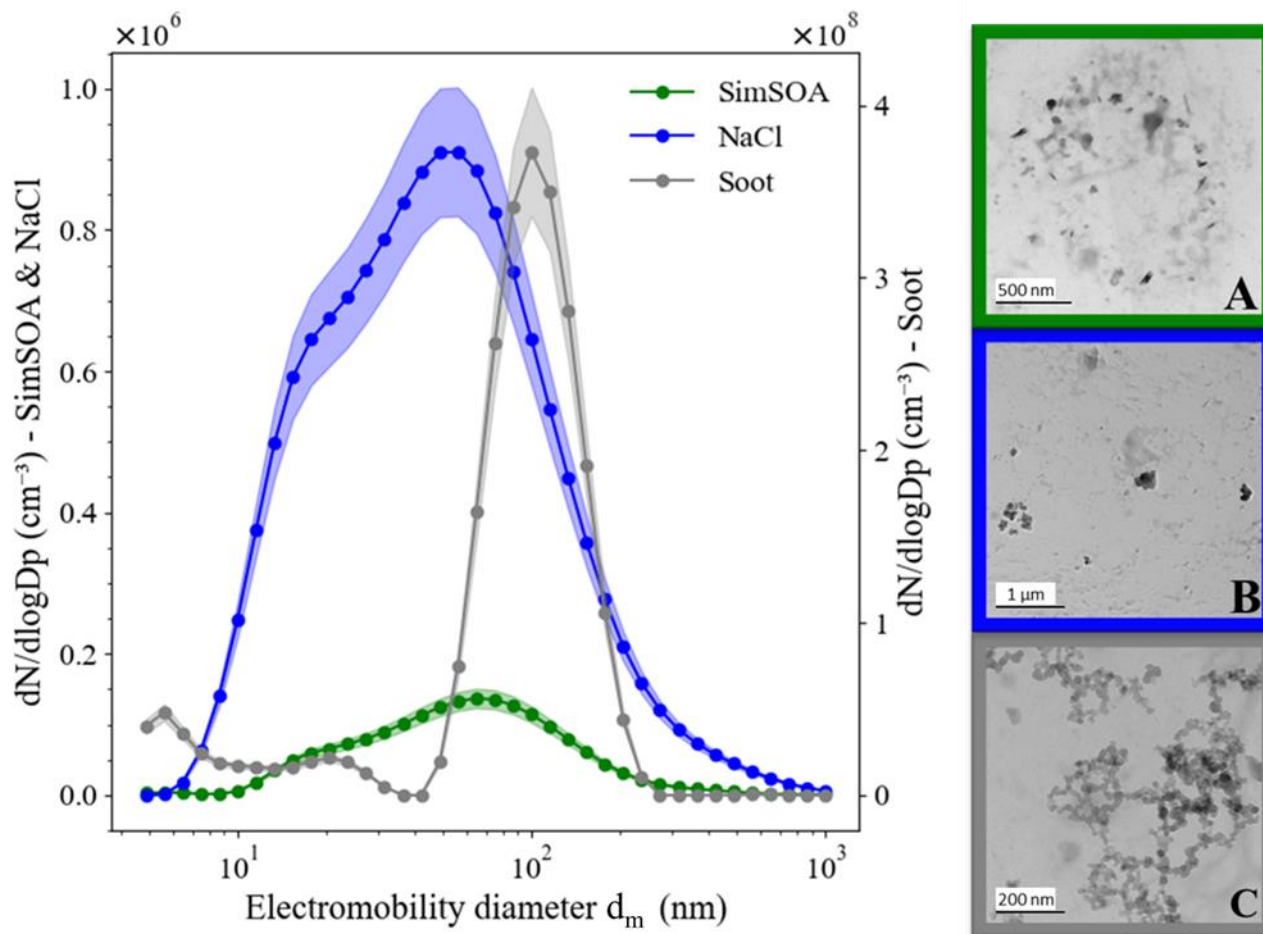
Figure 2: Particle number size distribution of three particle types for physical impactor testing - averaged for the duration of the experiments, and displayed with standard deviations for each particle type. The data for SimSOA (green) and NaCl (blue) are aligned on the left axis, while the soot data (black) is displayed on the right axis. SEM (Scanning Electron Microscopy) pictures of the test particles are displayed in Pictures A (SimSOA), B (NaCl), and C (Soot).

2.2.3 Determining physical parameters as evaluation criteria

To comprehensively characterize the four cascade impactors for UFP sampling, we focussed on determining the pressure-drop, cut-off properties, evaluating potential particle losses, and identifying any measurement artefacts that may arise. For each impactor we followed the same protocol: (step 1) determine the particle number size distribution of the test particles, (step 2) insert the (modified) impactor and monitor the transmitted particles as described, (step 3) conduct an "empty" measurement. For the "empty" measurements all nozzle stages and impaction plates were removed, so no size classification occurs, and inlet

and outlet of the impactor were connected just as in step 2. Step 3 allowed for baseline measurements without the influence of impaction stages while maintaining the set-up comparable to the transmission measurements of step 2.

Pressure-drop assessment: The pressure drop across each impactor was measured using a differential pressure gauge. This measurement encompassed the total pressure loss through the impactor, including the quartz fiber after-filter that was integrated within the system. For this measurement, T-junctions were installed at both the inlet and outlet of the impactor. Branches from these junctions were connected to the differential pressure gauge (HONEYWELL, 26 PCCFA6D Differential Pressure Sensor, relative, $\pm$ 15 psi) to record the pressure drop across the entire impactor and the quartz fiber filter on which the UFP are collected. The pressure drop was determined under the same flow rate that was used for each impactor under operating conditions.

Cut-off diameter determination: To derive the transmission of particles through the impactor as a function of their diameter, the ratio of the number concentration between the impactor (step 2) and the empty measurement (step 3) was calculated for each size bin. The resulting transmission curve was subsequently normalized for each impactor to the maximum transmission. From this, the dp50 values were deduced from a linear regression in the range of $30 < d_m < 110$ nm for NaCl and SimSOA particles and in the range of $60 < d_m < 110$ nm for soot. Additionally, we determined the steepness of the cut-off curve, and the dp90 and dp10 values, describing the diameters at which 90% and 10% of particles are deposited and not transmitted, respectively.

Evaluation of losses: We analyzed the transmission curves for the ultrafine section of the particle size distribution for evaluating the losses of each impactor. Due to the relatively larger uncertainties in the reference instruments for very small diameters, i.e. $d_m < 20$ nm, we decided to evaluate the particle number concentration at 30 nm for determining the losses in the ultrafine fraction. At this size all impactors showed a peak in the transmission curve which we used as a reference for determining the losses, calculated as 1 minus the derived transmission.

Observation of other artefacts: We also evaluated the transmission curve for other possible artefacts, as for example, for the transmission of larger particles, which potentially occurs as a result of particle bounce.

2.3 Overview of field application of the four cascade impactors for chemical analysis of organic markers in UFP

To assess the performance of the impactors under real environmental conditions, we operated all impactors simultaneously at the same location for the same duration for a side-by-side comparison. We took three samples of ambient aerosol on January 24th 2023, January 25th 2023, and January 30th 2023, in Bayreuth, Germany, for 24 hrs each. The impactors and their respective pumps were positioned indoors in the laboratories of the Bayreuth Center for Ecological and Environmental Research (BayCEER, 49.9305° N, 11.5881° E). The location is characterized by nearby manufacturing industries, road traffic,

and proximity to a highway, but also adjacent to residential areas of the city of Bayreuth with around 75,000 inhabitants (Bayerisches Landesamt für Statistik, 2022). Ambient air was drawn to each impactor through antistatic inlet lines each 1.2 m long (3/8", TSI). The lines, impactors and pumps were maintained at a constant temperature of about 21°C. Each inlet line was equipped with honeycomb ceramic bodies (25,4 x 50mm; 400 CPSI, Rauschert, Germany) coated with Sodium Thiosulfate (Merck, ReagentPlus®, 99%) right in front of the impactors' inlet. The coated ceramic body was hooded inside a stainless-steel housing and served as ozone denuder, preventing potential oxidation reactions on the already collected particles during sampling. The ozone scrubbers were previously evaluated for their capacity to scrub ozone from the sampling air and for potential losses ($\leq$ 6% for particles smaller than d_m=200 nm, $\leq$ 11% for particles larger than d_m=200 nm). Thereby, up to a concentration of 250 ppb ozone over 72 hours, ozone levels were reduced to below 5 ppb behind the ozone denuder. (Eckenberger et al., in preparation). The flow rate was adjusted before each measurement for each impactor.

All upper stages of the impactors were coated with a thin layer of vacuum grease (Apiezon L, Apiezon products, M&I Materials Ltd, Manchester, England) to ensure the adherence of deposited particles and minimize bounce. Therefore, we first dissolved vacuum grease in n-hexane (Merck, ReagentPlus®, ≥99%) and applied approximately 0.05 mL of this solution onto aluminiumfoils using a syringe. We allowed the solvent to evaporate for a minimum of 12 hours before mounting the treated foils onto all existing stages of the 120R MOUDI, the ultraMOUDI, and the ELPI. For the PENS, which does not have an impaction plate suitable for filter installation, the grease was applied directly to the plate following the evaporation process. After each 24-hour sampling period, all impactor and nozzle plates were cleaned using an ethanol-water mixture, then dried with synthetic compressed air, and recoated before the next measurement. For collection of UFP, we inserted pre-baked quartz fiber filters (Whatman QM-H, 47mm or 37mm) in the after-filter holder of each impactor, pre-baked at 300°C for 24h. These were stored at -20°C immediately after collection.

For comparing the results of chemical analysis of the sampled UFP between the four impactors, we selected six organic marker components to encompass a mixture of anthropogenic (Benzo[a]pyrene (BaP), Benzo[b]flouranthene (Bbf)) (Hussain et al., 2018) and biogenic sources (Pinic acid (PA), Terpenylic acid (TA) (Vestenius et al., 2014)). Furthermore, we analyzed Levoglucosan (Levo) as marker for biomass burning (Simoneit et al., 1999)and N-(1,3-dimethylbutyl)-N'-phenyl-p-phenylenediamine (6PPD) as marker for tire wear material (Klöckner et al., 2021). The marker components were selected to provide a diverse range of molar masses, volatility, and mass abundance.

2.3.1 Extraction of samples

We extracted the selected marker components from the filters via a soft, solvent-based and optimized protocol: (1) the filter loaded with particles was divided into two equal parts. One part was extracted, the other one used as backup. (2) The filter-half for extraction, was spiked with 50 µL of each internal standard, namely 3-Methylcholanthrene (3-MC, 0.4 µM) and

365 Nicotinic acid (NA, 10 µM) and cut into small fragments. (3) These filter fragments were then transferred into a glass container with a screw cap, and 2 mL of extraction solvent (e.g. analytical-grade Dichloromethane (DCM, Fisher Chemical, 99.8%) and Methanol (MeOH, Carl Roth, ≥ 99.9%)) were introduced. (4) The samples underwent extraction through agitation within a closed flask for a duration of 15 minutes using a vortex shaker (2000 rpm). (5) Filter residues were kept in the glass container. Extracts were filtered using specially designed glass frits with a diameter of 1 cm and a pore size of 20 µm to eliminate any

370 potential filter residue.

Steps (3) to (5) were repeated three times, each time employing a different extraction solvent. The sequential solvents used were, in order, pure MeOH, 50:50 MeOH:DCM, and pure DCM. Subsequently, the solvent from the combined extracts was evaporated under a gentle flow of Nitrogen (N_2, 99.99%) while cooled with ice to avoid loss of semi-volatile compounds. A

375 droplet was kept as residue, approximately 0.5 µL in volume, which was dissolved in 1 mL of a 60:40 solution of Acetonitrile (ACN, Carl Roth, 99.95%) and water (H_2O, obtained from Seralpur PRO 90 CN system with Supor DCF filter, Electronics Grade, 0.2 µm). This was transferred into a separate vial for subsequent analysis. Throughout the entire sample preparation process, the samples were stored in an ice cooled environment.

2.3.2 HPLC analysis for chemical marker profiling

380 The analysis of the sample extracts was performed at two High Performance Liquid Chromatography (HPLC) systems. For the detection of PA, TA, Levo, and 6PPD, an Agilent series 1100 chromatograph equipped with an electrospray ionization mass spectrometer (ESI-MS, Agilent 6130 single quadrupole) was utilized. To determine the concentration of the polycyclic aromatic hydrocarbons (PAH), BaP and Bbf, an Agilent 1260 Infinity system coupled with a fluorescence detector (FLD, Agilent 1100 Series) was employed. For the mobile phase, HPLC-grade acetonitrile, water, and formic acid as buffer (HCOOH,

385 Carl Roth, p.a. ≥ 98%) was used. We applied three different methods which are summarized in Table S1.

To assess the efficacy of the sample preparation, including the extraction method, recovery experiments were conducted in triplicates. Half of the pre-heated quartz fiber filter (Whatman QM-H, 47 mm) was spiked with 10 µL of a 10 µM standard solution encompassing all markers. Subsequently, the spiked filter was extracted as outlined previously. The recoveries (Rec)

390 were ascertained utilizing external standard (ESTD) calibration and calculated by dividing the measured concentration of each marker by the expected (spiked) concentration.

$$\text{Rec} = \frac{c_{\text{measured}}}{c_{\text{expected}}} \cdot 100 \qquad (1)$$

395

13

The obtained recoveries were as follows: BaP 78±7%, BbF 74±7%, Levo 79±7%, PA 84±8%, TA 85±8%, and 6PPD 75±7%. As these recovery rates describe the average systematic loss of the marker compounds during extraction, we corrected our data using the following equation:

$$c_{sample_{corrected}} = c_{sample_{measured}} \times \left(\frac{100}{Rec}\right) \tag{2}$$

The recovery-corrected results were then validated against the NIST standard (SRM 2786, <4 µm) which was applied to a filter, extracted and analysed according to the methods described herein, for validation and showed agreement within the uncertainty of the measurement, even in the presence of a particulate matrix. The limit of detection (LOD) was determined based on the standard deviation (σ) of the response from a modified calibration solution, targeting a signal-to-noise ratio of approximately 3 for each analyte, as well as the slope/response factor (RF) from the ESTD calibration.

$$LOD = \frac{3 \cdot \sigma}{RF} \tag{3}$$

The LOD was calculated across four replicates. Furthermore, the LOD for airborne concentrations (LOD_{Air}) [pg/m^3] was calculated by dividing the LOD by the sampling volume. For the MOUDI and ELPI devices sampling for 24h with 30 L/min, the sampling volume was 43.2 m³. For the PENS, which has a sampling flow of 4 L/min, the sampling volume was 5.76 m³. The LOD values ranged around 1-2 and 40-186 pg/m³ for target markers measured with HPLC-FLD and HPLC-MS, respectively. The LOD increased by a factor of 7.5, when sampling a smaller volume as for the PENS compared to all other impactors (Table S2, Supporting information). Additionally, we estimated impactor-specific overall measurement uncertainties using Gaussian error propagation, with uncertainties ranging from 13.8% to 17.8% (SI 1.1). This estimate for the uncertainty includes the instrumental variability for repeated analysis (2%), reference material uncertainty (0.5%), preparations of stock solutions (5%), dilution errors (5%), inaccuracies in volume determination (1%). Additionally, it accounts for impactor-specific factors, including flow adjustment errors (3–10%) and handling errors (10–15%).

14

3. Results and Discussion

3.1 Physical characterization I: pressure drop, cut-off diameters, steepness of cut-off curve

The **pressure drop** across an impactor including the quartz fiber filter can significantly influence the collection efficiency and the chemical composition of the captured particles. The more the pressure drops across the impactor and quartz fiber filter, the higher the rate of potential evaporation of semi-volatile compounds. For the four tested impactors, the pressure-drop was 260 ± 1 (PENS), 420 ± 2 (ultraMOUDI), 600 ± 3 (120R-MOUDI), and 690 ± 3 (ELPI) hPa.

Figure 3 shows the normalized transmission curves obtained from testing the four impactors with the three test particle mixtures. **Cut-off** diameter**s** were calculated as dp50 for the electromobility diameter. They increased consistently for all impactors from NaCl particles over SimSOA to soot particles (59-68 < 70-74 < 102-116 nm). The best agreement between the individual impactors' cut-off diameters was found for SimSOA. For SimSOA, the ultraMOUDI and 120R MOUDI had the smallest cut-off diameter with an electromobility diameter of 71 ± 7 and 70 ± 7 nm. Contrastingly, for soot, the largest deviations among the impactors' cut-off diameter were found, showing that the devices deviated about 14 nm at most. Here, the two MOUDI-models had highest cut-off diameter and the PENS the smallest one with 102 ± 10 nm. For NaCl and SimSOA particles, we compared the aerodynamic cut-off diameters, which were 86 ± 9 and 84 ± 8 (ultraMOUDI), 89 ± 9 and 85 ± 9 (120R MOUDI), 99 ± 10 and 89 ± 9 (PENS), and 100 ± 10 and 85 ± 9 (ELPI) nm for NaCl and SimSOA, respectively. For the calculation, a shape factor of 1.0 and a density of 2.165 g/cm³ were used for NaCl, while a shape factor of 1.2 and a density of 1.21 g/cm³ were applied for SimSOA.

Generally, the transmission curves were steeper for soot than for SimSOA than for NaCl particles. This trend is strongest for ELPI and PENS, which have the highest **steepness** for soot with slopes of the transmission curve of -1.1 1/nm and the least sharp cut-off curve for NaCl with -0.52 and -0.56 1/nm, respectively. The sharpness of cut-off curve of the 120R MOUDI and ultraMOUDI seems less sensitive to the type of test particle, as the steepness of the transmission curves varied about 9% at most between the different test particles. The four impactors had best agreement regarding the steepness of the transmission curve for SimSOA with a relative difference between maximum and minimum slopes of about 26%.

The **dp10 and dp90** represent the diameters at which 10% or 90% of the test particles were deposited on impaction plates of the impactor. An impactor with closely spaced dp10 and dp90 values would have a steeper transmission curve, indicating a more precise segregation of particles by size. For all impactors, the lowest dp10 values were observed with NaCl particles ($dp10_{ave}=34$ nm, average across all impactors). The dp90 did not vary systematically between the test particles and impactors ranging from 125 ± 13 nm (for NaCl particles collected with ultraMOUDI) to 183 ± 18 nm (for SimSOA collected with 120R MOUDI). As this general trend might be driven by the relatively sticky nature of NaCl particles and SimSOA leading to a

15

relatively smeared cut-off curve, it is interesting to observe the sharpest cut-off curve for the soot particles, which exhibit the most complex shape of the three tested particle types. This can be seen also from the difference between dp90 and dp10, which was smallest for soot particles for all four impactors.

SimSOA is likely the most representative test particle for environments ranging from urban to suburban to rural which are not coastal, kerb site or subject to nearby combustion sources. For the tests with SimSOA, the four impactors performed comparably in terms of cut-off diameter, transmission curve steepness, and dp10 and dp90 (Table 1). We observed a tendency for a sharper separation of UFP with PENS and ELPI compared to the two MOUDI-models. However, relatively larger deviations between the four impactors were observed for soot particles, both in cut-off diameter and steepness. The estimated aerodynamic cut-off diameters for SimSOA and NaCl overlap for all the impactors within their uncertainties in a range of 84-100 nm. Typically, the UFP range includes the nucleation mode and marks the shoulder of the accumulation mode. With the perspective of a mass based analysis, particle composition of these two modes would be reflected in the results. Yet, as the mass of particles around 100 nm is small, the observed variations in cut-off diameter likely do not diminish their comparability.

Table 1: Summary of performance test results for the four impactors and the three test aerosol mixtures. The dp values are provided as electromobility diameter in nm. The steepness describes the slope of the transmission curve around particles diameters of 100 nm. The dp50$_a$ (aerodynamic particle diameter at 50% collection efficiency) is calculated as aerodynamic cut-off diameters derived for the salt particle tests.

| Impactor	Aerodynamic cut off [nm] (manufacturer)	Aerosol type	dp value [nm] 10	dp value [nm] 50	dp value [nm] 90	Steepness [1/nm]	dp50$_a$ [nm]
120R MOUDI	100	NaCl	34±4	61±6	182±18	-0.55	89±9
		SimSOA	41±4	71±7	183±18	-0.55	85±9
		Soot	78±8	116±12	175±18	-0.86	/
PENS	100	NaCl	30±3	67±7	177±18	-0.52	99±10
		SimSOA	42±4	74±7	148±15	-0.64	89±9
		Soot	69±7	102±10	153±15	-1.1	/
ELPI	90	NaCl	39±4	68±7	162±16	-0.56	100±10
		SimSOA	39±4	71±7	148±15	-0.65	85±9
		Soot	72±7	106±10	162±16	-1.1	/
ultra MODUI	100	NaCl	32±3	59±6	125±13	-0.67	86±9
		SimSOA	35±4	70±7	162±16	-0.58	84±8
		Soot	76±7	112±11	166±17	-0.95	/
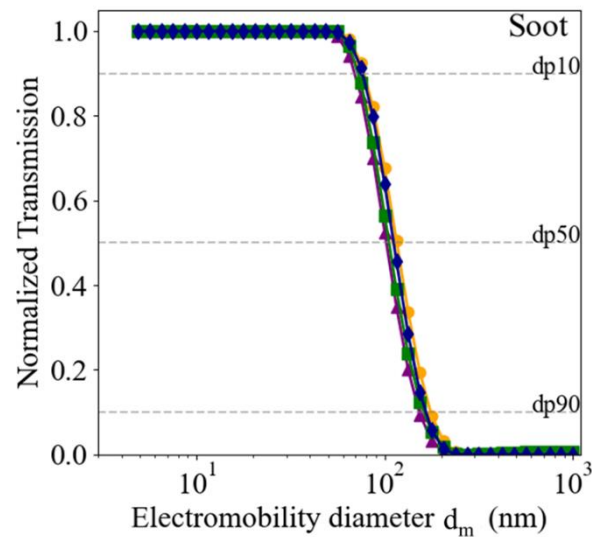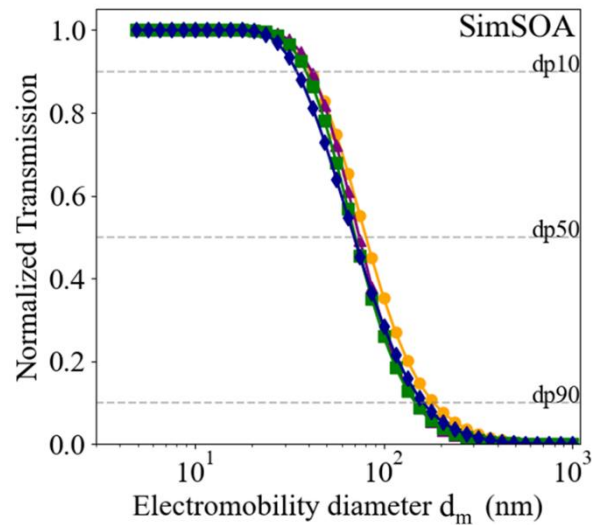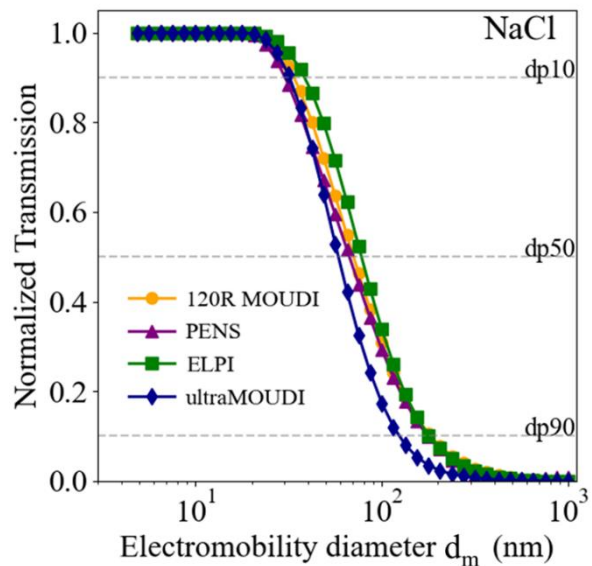
Figure 3: Normalized transmission curves across three test particle types including NaCl, SimSOA, and soot, as captured by different impactors: 120R MOUDI (orange, circle), PENS (purple, triangle), ELPI (green, square), and ultraMOUDI (blue, diamond markers). Each subplot displays the transmission versus electromobility diameter (nm) on a logarithmic scale. Lines are included to guide the eye.

485

3.2 Physical characterization II: losses and particle bounce
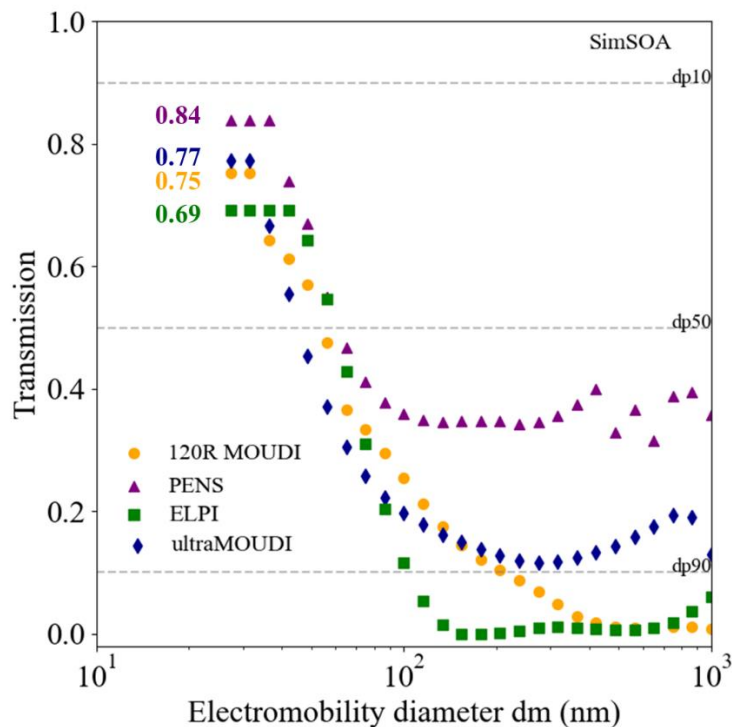
Figure 4: Transmission curves for the four tested impactors collecting SimSOA generated within the atmospheric simulation chamber. Note that all tests were performed without applying coating. The four impactors are marked as 120R MOUDI (orange, circle), PENS (purple, triangle), ELPI (green, square), and ultraMOUDI (blue, diamond markers).

For determining potential **losses** within the impactors, we compared the transmission curves for SimSOA generated in the atmospheric simulation chamber (Fig. 4). The maximum transmission in the ultrafine fraction at 30 nm was 84±8% for PENS, 77±8% for ultraMOUDI, 75±8% for 120R MOUDI, and 69±7% for ELPI. These results indicate that the ELPI had the highest losses of SimOA UFP during sampling compared to the other tested impactors. However, considering the overlap of uncertainties, these differences are not significant. Losses can be due to wall losses or interstage losses, retaining particles on surfaces other than the impaction plate. In addition, losses can also occur through evaporation of (semi) volatile particles, especially under high pressure drop during flow-through (Marple and Willeke, 1976; Won Kim, 2010).

500

Ideally, the transmission should ultimately reach zero for particles with larger diameters, as these should be retained in the upper stages of the impactor. However, the elevation for diameters between 200 and 1000 nm above zero suggests the occurrence of **particle bounce** (Fig. 4). The ELPI detected very few particles at the larger diameters, with minimal transmission observed for these particle sizes. Thus, within the uncertainty, no particles with an electromobility diameter larger than 177

505 nm passed the last impaction stage. A similar observation can be made for the 120R MOUDI, where very few particles were detected at larger diameters, approaching minimal transmission at an electromobility diameter of 562 nm. For larger particles, the transmission remained zero. This is in line with the comparably flat slope of the transmission curve of the 120R MOUDI, indicating a broad separation of particle sizes rather than a sharp cut-off curve (Table 1). However, both PENS and ultraMOUDI had notable bounce effects. For the PENS, the transmission dropped to a local minimum at 133 nm

510 (electromobility diameter) and remained at approximately 38% for larger particles. For the ultraMOUDI, the local minimum of transmission was at an electromobility diameter of 273 nm with 13%, but then increased again for larger particle diameters to about 19%.

Overall, the impactor design seems to critically impact potential losses and particle bounce. The ELPI and the 120R MOUDI

515 have a higher number of stages, impaction and nozzle plate pairs, before ultimately separating UFP (13 and 9 stages, respectively), when compared to ultraMOUDI and PENS (3 and 2 stages, respectively). The increased number of stages appears to reduce the bounce effect (Fig. 4). This is likely because particles have more opportunities to impact as they traverse through multiple stages, with each stage being less loaded with particles, reducing the probability of bounce. As both ELPI and MOUDI are modular cascade impactors, they allow to include a different number of stages with different cut-off diameters,

520 which in turn might result in different sampling characteristics not only for the ultrafine but also for the upper stages. However, including a higher number of upper stages could come at the cost of comparably increased losses in the UFP range.

Here, the losses in the UFP range were similar for ELPI, 120R MOUDI and ultraMOUDI. This contrasts with the PENS, which had the smallest loss amongst all tested models with about 6%, likely due to its design with the cyclone pre-separator and only

525 one nozzle plate. We can compare our results to a few other studies, that experimentally determined the loss rate of the MOUDI. Liu et al. (2013) showed a total loss of a MOUDI (Model 110) in the range of 2.9-26.1% increasing with decreasing dp50, which was attributed mostly to convective-diffusion. Similarly, Durand et al., (2014) observed losses by convection-diffusion in cascade impactors with stages designed for ultrafine particles below 100 nm. Ungeheuer et al. (2022) measured losses of 28% and 40% in the Nano-MOUDI (110) for particles with aerodynamic diameter of 32-56 nm and 18-32 nm, respectively. It

530 is thought that diffusion deposition becomes increasingly significant for smaller particles, which can lead to substantial particle losses. As high uncertainties are associated with both MPSS and DMS, when measuring particles with diameters below 20 nm, we could not test this behaviour within out setup. However, a mass based analysis of UFP might be less affected by such losses than the measurement of the number concentration.

20

535 It has been reported, that particle bounce becomes particularly significant for lower cut-off stages because of the gradual reduction in pressure at each stage, which subsequently leads to a decrease in relative humidity (RH). The reduction in RH in turn can intensify the particle bounce effect (Chen et al., 2011). Pressure dropped most drastically throughout the ELPI, which could be problematic for collecting semi-volatile organic marker compounds (Yao et al., 2022). Knowing that the diameters of cut-off and the effective sharpness of the separation between fine and ultrafine SimSOA particles were comparable for all

540 tested impactors, the impact of losses and particle bounce on a mass based chemical analysis might be significant, which therefore is further investigated in the following.

Considering the mass of UFP compared to the mass of potential artefacts, we wanted to understand the relative impact of particle bounce. Even a few larger particles or fragments bouncing onto the UFP collection substrate could heavily skew the

545 results, leading to an overestimation of the UFP mass concentration and a misrepresentation of their chemical composition. This is particularly problematic because UFP can have different chemical properties and health impacts compared to larger particles (Abdillah and Wang, 2023; Müller et al., 2012). Particle bounce-off can be influenced by the impaction surface, the presence, type and depth of a coating, particle types, particle loading, sampling conditions, and the impaction substrate. Particularly during long-term sampling with heavy particle loads, deposited particles were found in excessive layers (Kulkarni

550 et al., 2011; Marple et al., 1991; Pak et al., 1992; Turner and Hering, 1987; Chang et al., 1999; Newton et al.;Lai et al., 2008; Rao and Whitby, 1978).

To test whether increased particle load leads to more severe particle bounce, we varied the particle number concentration in the chamber for SimSOA from a maximum of about 200,000 cm^{-3} to a more realistic maximum of about 5,700 cm^{-3} (see Figure

555 5). As a wide range of number concentrations was covered, we measured the particle number size distributions with both, DMS500 (Level 1, in Fig. 5a) and MPSS (Level 2, 3, and 4, in Fig. 5a). Additionally, Figure 4a presents an exemplary number size distribution (Level 4) for ambient particles which was collected during the period of environmental sampling when the impactors were deployed side-by-side (see 2.3. For these levels, Figure 5b shows the transmission through the PENS impactor as an example. Indeed, reducing the particle number concentration resulted in a decreased bounce effect, although it remained

560 noticeable. Compared to the highest particle load (Level 1), transmission was reduced in Level 2 for particles sized 150-200 nm, while particles > 500 nm still exhibited transmission rates of up to 34%. Level 3a was the relatively lowest particle load, which then decreased transmission to about 5-9% remaining relatively consistent across the diameter range of 170-800 nm.

Furthermore, greasing of upper stages is a method that has previously been suggested and applied to reduce particle bounce

565 (Baron and Willeke, 2011; Ungeheuer et al., 2021). To test this method, we greased the upper stages of the PENS (Fig. 4 right panel, Level 3b). The application of the coating on the impactor further reduced the bounce effect, lowering transmission rates to 0-6% within the same particle size range. The duration of these measurements is notably brief (20 minutes), in contrast to

the typical collection times employed with impactors (e.g. 24 hr). Thus, we greased also the upper stages of the 120R MOUDI and monitored the transmission on three consecutive days while sampling ambient air. While the greasing improved the

570　sharpness of the cut-off curve, the transmitted fraction of particles around a size of about 200 nm increased during the three days from about 0 to 15%. These tests highlight the variations in the observed bounce effects over short and extended collection periods, which may be very much dependent on particle load and nature. Yet, greasing the upper impaction stages overall improved the UFP sampling as it reduced the fraction of relatively larger particles being transmitted.
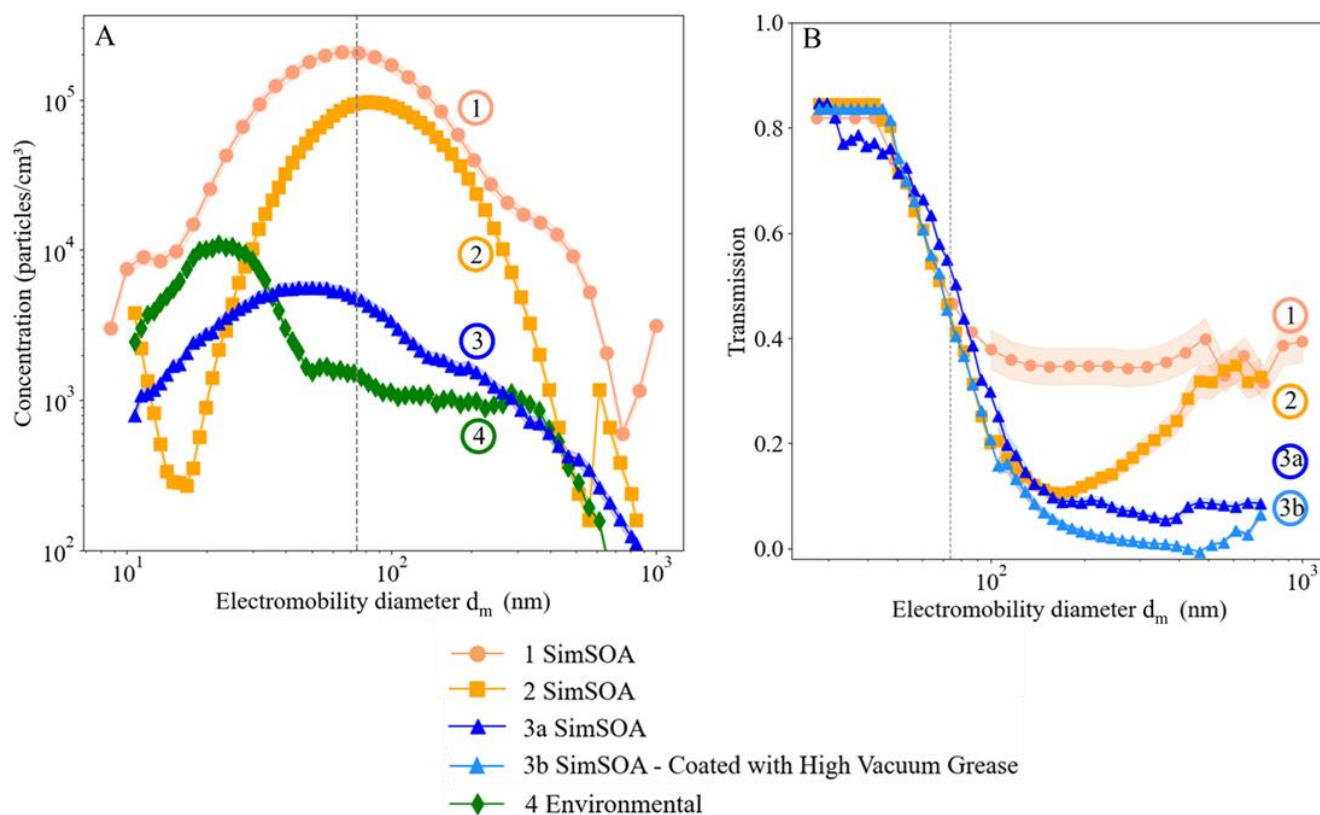
575

Figure 5: A illustrates the particle number size distribution in units of particles/cm³ for SimSOA (1, as detected in highest concentrations with DMS500, 2 and 3, in relatively lower concentrations measured by MPSS), and environmental SOA (4). B delves into the transmission curves of the PENS for the respective particle size distribution. Data labeled with 3a and 3b display uncoated and coated measurments using high vacuum grease.

580　**3.3 Physical characterization III: transmitted particle mass**

Typically, UFP collection using impactors is followed by the analysis of the chemical composition which have a mass based focus. Breakthroughs of coarser particles into the UFP range can significantly distort mass based analytical results, as particle mass increases in cubic proportion to the diameter. As an example, Figure 6 illustrates the transmission of particles through

the PENS based on their respective mass. The density of the alpha-pinene particles was measured by Zelenyuk et al. (Zelenyuk et. al., 2008) as 1.20 g/cm³. We used this value to calculate the mass of particles transmitting the impactor according to the measured number size distributions assuming spherical shapes of the SimSOA particles. We separated the data into two size classes (based on the particle's electromobility diameter): (1) the entire recorded range 10-800 nm and (2) the UFP range 10-74 nm which is below the previously determined dp50 (section 3.1).

The set of measurements includes particle mass as measured directly from the chamber, from the empty PENS, the uncoated PENS, and the coated PENS (Fig. 6). The total mass of all particles in the chamber ranging from 10 to 800 nm, calculated directly from the measured particle number size distribution, was 220.2 µg/m³. Due to losses in the lines and the empty PENS, the mass was reduced to 205.87 µg/m³. Upon separation, 21.4 µg/m³ were transmitted through the PENS when no coating was applied. Through the coated PENS a particle mass of 3.3 µg/m³ was transmitted. This highlights the coated impactor's capability to retain over 98.5% of the test particle mass, whereas the uncoated impactor captured only approximately 90.3%. The difference are artefacts due to bounce and fragmentation of larger particles sampled as UFP. Figure 6 shows also, that the transmitted ultrafine fraction as detected with MPSS remained comparable between coated and uncoated tests. For this test, we chose a reduced particle number concentration, compared to the above cut-off characterizing experiments, and SimSOA particles in the context of environmental measurements. Due to the nature of SimSOA they are likely not representative of a worst-case scenario for particle bounce.
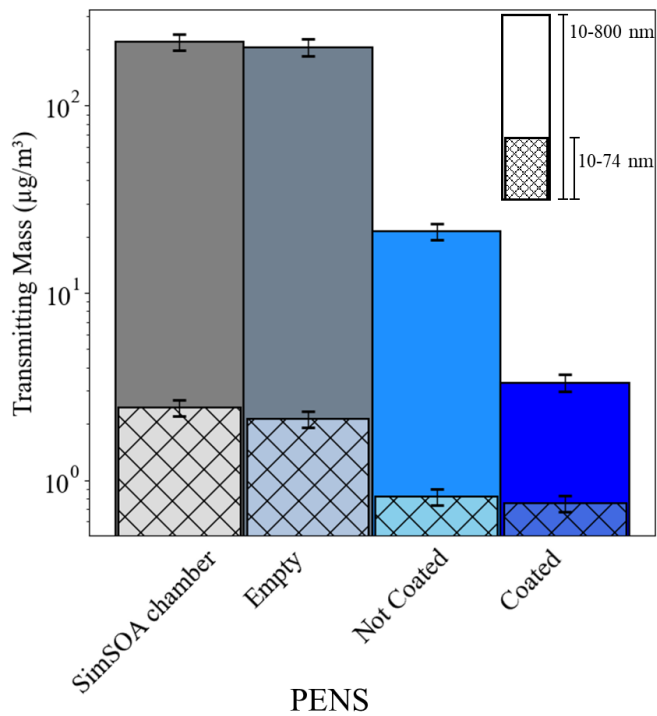
Figure 6: Comparative bar chart displaying the mass of transmitting particle mass in µg/m³ for coated and not coated PENS tests compared with the original aerosol mixture (SimSOA) and the empty PENS. Two segments present the entire observed electromobility diameter range (10...800 nm) and ultrafine fraction (10...74 nm). The chart employs a logarithmic scale on the y-axis.

24

3.4 Field application: chemical analysis of organic markers

We evaluated the performance of the four cascade impactors under environmental conditions with six selected markers (cf. methoden):

- Polycyclic aromatic hydrocarbons (PAH) have potential impact on human and environmental health (Hussain et al., 2018; Kim et al., 2013; Wang et al., 2006). **Benzo[a]pyrene** (**BaP**, M= 252.31 g/mol) and **Benzo[b]fluoranthene** (**BbF**, M= 252.31 g/mol) are high molecular weight PAHs with five aromatic rings, low volatility and predominantly found in fine particulate matter originating from incomplete combustion.

- **Levoglucosan** (**Levo**, M = 162.14 g/mol) is a well-studied tracer for cellulose combustion (Bhattarai et al., 2019; Simoneit et al., 1999). Its presence is indicative of sources like residential wood burning, agricultural fire practices, and wildfire emissions. Levoglucosan is semi-volatile and can partition between gas- and particle-phase (Xie et al. ,2014).

- **Pinic acid** (**PA**, M = 186.21 g/mol) and **terpenylic acid** (**TA**, M = 198.24 g/mol) are representative of secondary organic aerosol (SOA) from biogenic origin, produced through the oxidation of terpenes such as alpha-pinene and beta-pinene, which are emitted by vegetation. (Claeys et al., 2013; Grieshop et al., 2007).

- **N-(1,3-dimethylbutyl)-N'-phenyl-p-phenylenediamine (6PPD,** M=268.40 g/mol) is an additive in tire wear materials and has recently been proposed as a tracer for non-exhaust traffic-related particles (Chen et al., 2023; Hu et al., 2022).
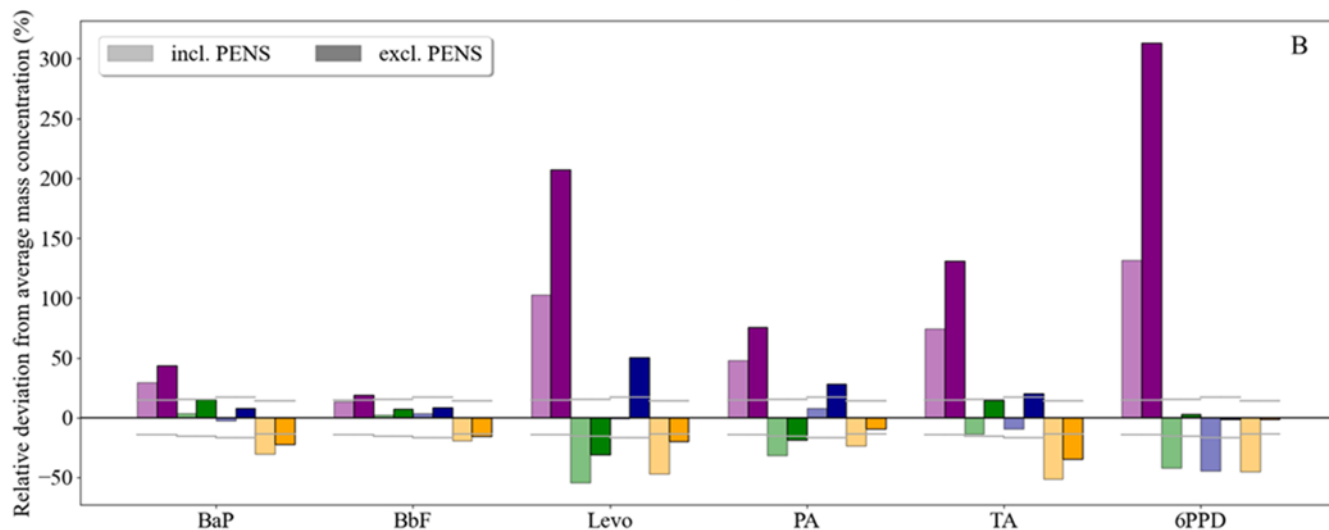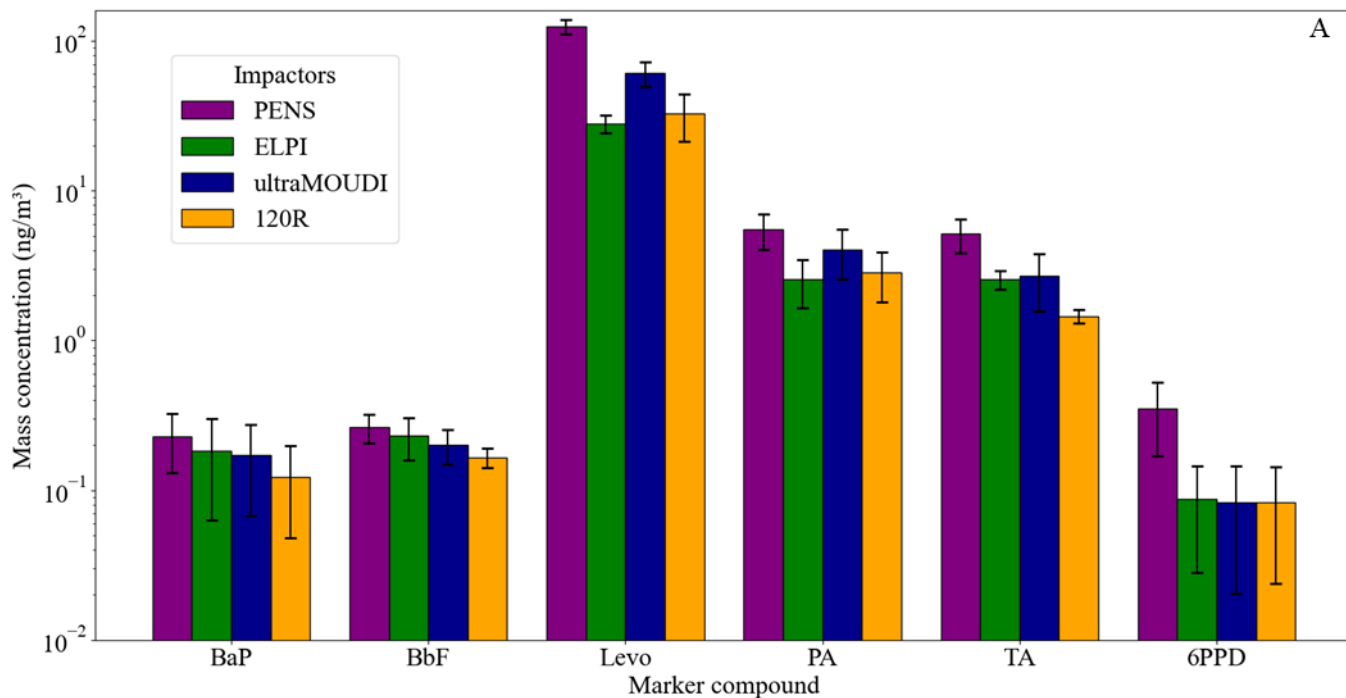
Figure 7: A : Bar chart showing the average mass concentration of selected organic marker compounds in UFP collected with PENS (purple), ELPI (green), ultraMOUDI (dark blue), and 120R MOUDI (orange) of three days in ng/m³ on a logarithmic scale. Error bars indicate standard deviations. B: Relative deviation (%) in mass concentration of BaP, BbF, Levo, PA, TA, and 6PPD in UFP from the average of all impactors including and excluding PENS for the caluculation of the average (transparent/opaque bars). For comparison, horizontal grey lines represent the estimated overall error for each marker and impactor (SI 1.1). A logarithmic representation of 7b can be found in SI Fig 2.

We analyzed UFP sampled in an urban, semi-industrial environment. The observed average mass concentrations are presented in Figure 7A. Furthermore, we evaluated the relative deviation of each impactor compared to the average of all impactor results

(Figure 7B). Overall, the best agreement between all impactors was found for the two PAHs. For BaP, the average mass concentration was highest for the PENS with 227.2 ± 97 pg/m³ (average ± standard deviation over the three consecutive days), which is 29% above the average of 175.65 pg/m³ when considering all impactors. ELPI and ultraMOUDI agreed with about 4% above and 3% below the average, respectively. The 120R MOUDI had the lowest average concentration with 122.6 ± 74 pg/m³, which was 30% below the overall average. For BbF, the tendencies were the same but less pronounced. We can highlight two findings here for the analysis of the two PAHs: Firstly, the maximum disagreement can be as large as 59% between PENS and 120R MOUDI. Secondly, the two PAHs, originating from the same sources and found in >90% particle phase, exhibit the same sampling tendencies across the impactor models. This is likely due to their identical molecular weights and very comparable boiling points.

As the results of the PENS seemed to be consistently on the higher end for all marker compounds, we calculated the average between all impactors including and excluding the PENS and then compared (Figure 7B). The PENS exceeded the average of the remaining impactors by a factor of 1.3 for BaP, 1.2 for BbF, 2.0 for Levo, 1.5 for PA, 1.7 for TA, and 2.3 for 6PPD. Our cut-off characteristic tests indicate three potential reasons for this overestimation. Firstly, the PENS had the lowest pressure drop of all impactors (260 hPa), which might affect the gas-particle partitioning of semi-volatile compounds in a way that e.g., Levo, TA, and PA had comparably higher mass concentrations in PENS samples. Secondly, the bounce effect was more pronounced in the PENS and dependent on the particle number concentration of the SimSOA. Possibly and despite the applied coating, the overestimation in marker mass concentrations of the PENS could be due to a bounce effect, which is increasing with rising ambient mass concentrations. Thirdly, the physical loss in the UFP range was relatively small in the PENS when compared to the other impactors (Figure 4). The losses, however, were similar in all impactors and likely less impactful from a mass-based viewpoint.

The comparison of the remaining impactors showed the best agreement for the results of 6PPD. Herein, the two MOUDI models had on average 83±30 pg/m³ and the ELPI 86±48 pg/m³ of 6PPD in the sampled UFP. The differences amongst the 120R MOUDI, ELPI, and ultraMOUDI increased from 6PPD (-2 to +3%), to PAHs, BaP and BbF, (+8 to -22%), the organic acids, PA and TA, (+20 to -35%), and, Levo (+51 to -31%). Thus, the range of deviation increased with the average observed mass concentration from 6PPD (84±30 pg/m³), to BaP (158±25 pg/m³) and BbF (199±23 pg/m³), to PA (3,144±620 pg/m³) and TA (2,231±541 pg/m³), and finally to Levo (40,660±17,148 pg/m³).

It should be noted that the differences among the impactors fall within the same order of magnitude as the overall uncertainty for most markers (BaP, BbF, TA, and PA). Yet, these differences were systematic and seem to not only depend on the impactor design but also on the properties of the analyzed compounds (see 2.3.2).

3.5 Influence of physical factors on the results of the marker mass concentration analysis in UFP

We analyzed systematically the influence of the previously examined physical factors on the results of the marker concentration in UFP with respect to the markers properties. While the cut-off diameter, cut-off curve steepness and losses seem to not vary largely between the four tested impactors, the pressure drop (mass loss) and the effect of particle bounce (mass gain) have the potential to drive the observed differences of the mass based UFP analysis.

We expected the pressure drop to primarily affect the semi-volatile markers, PA, TA, and Levo, due to evaporation losses during sampling. Figure 8a illustrates the dependency of the absolute deviation of the average mass concentration on the pressure drop for all samples and impactors. The absolute deviation of the average mass concentrations of PA, TA, and Levo decreased with increasing pressure drop, stronger than the less volatile markers, BaP and BbF. We lumped these two groups of markers, semi-volatile and mostly particle-bound, and compared the change in concentration for the two extremes, the PENS with the smallest pressure drop (260±1 hPa) and the ELPI with the largest pressure drop (690±3 hPa). The lower-volatility markers (BaP,Bbf) decreased in average concentration about 15%. In contrast, the average mass concentration of the higher-volatility markers (PA, TA) decreased about 52%. These findings seem to confirm that the larger pressure drop in the impactors leads to evaporation and thus a mass loss of the semi-volatile substances. Likely, the evaporative loss depends also on the collection substrate. When sampled in QFF, for example, UFP are exposed individually and ventilated efficiently. However, here QFF was used in all impactors for UFP sampling and. Furthermore, we firstly noted differences between 120R MOUDI and ELPI, despite of a comparable pressure drop. Secondly, mass concentrations of 6PPD were comparable for all impactors except for the PENS. These observations indicate additional influencing factors beyond the pressure drop alone, which could potentially affect the analysis more significantly.

Despite the application of a coating, we suspected particle bounce and thus tested whether the absolute deviation from the impactor average mass concentration was dependent on the ambient marker mass concentration (Fig. 8b). While we expected an increasing effect with higher mass concentrations, any potential dependency became more apparent only at the highest daily average concentrations, particularly above 1 ng/m³. Below this level, the data primarily exhibited scatter, suggesting that any systematic influence of particle bounce may be less pronounced at lower concentrations. Yet, any potential dependency could only be seen in our data for the highest daily average concentrations, particularly above 1 ng/m³. Below this level, the data do not suggest any systematic influence of particle bounce.

While the nature of the particle could play a role in its efficiency of being captured in the filter substrate - such as comparing sticky, spherical SOA to combustion particles with complex shapes (Boskovic et al., 2005; Matthew et al., 2008; Huang et al., 2004) the design of the impactors likely determines the potential for particle bounce. The main difference between the PENS and the other impactors is the cyclone and the number of stages used for separating and impacting larger particles. The larger number of stages and, thus, the larger number of coated surfaces in the two MOUDI models and the ELPI are likely beneficial for reducing the impact of particle bounce. The rotating stages of the 120R MOUDI potentially played a more significant role

in the field study with longer sampling times than in laboratory tests. Over time, the rotation resulted in an even loading of the upper stages, which in addition to the coating likely reduced particle bounce. Thus, we observed quasi no dependency of the 120R MOUDI deviations from the average mass concentration with increasing mass concentration (Fig. 8b). However, as the marker compounds with a high observed mass concentration are at the same time semi-volatile, we cannot completely separate the two effects of pressure drop driven losses and mass gain due to particle bounce within this study.
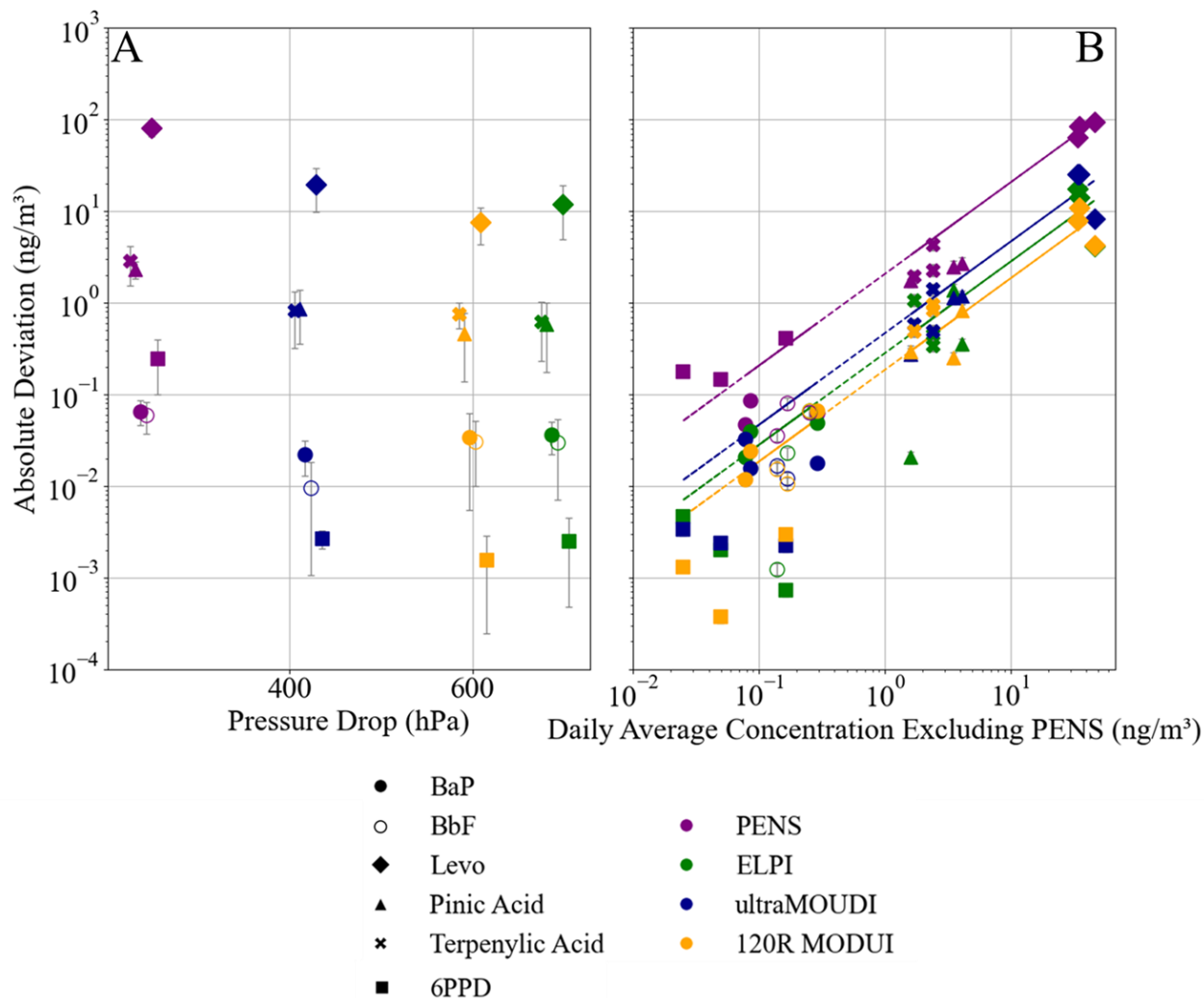
Figure 8: (A) Absolute deviation of average mass concentrations of BaP, BbF, Levo, Pinic Acid, Terpenylic Acid, and 6PPD as determined with the four impactors as a function of pressure drop across the impactors. Data points are displaced horizontally around each impactor's nominal pressure drop value for reasons of illustration to allow comparison while avoiding overlap. Markers denote different substances: BaP (filled circle), BbF (unfilled circle), Levo (diamond), Pinic Acid (triangle), Terpenylic Acid (X), and 6PPD (square). (B) Absolute deviation from the mass concentration average for PENS (purple), ELPI (green), ultraMOUDI (dark blue), and 120R MODUI (orange) for the selected organic marker compounds in UFP. Linear regressions through the origin are included for each impactor, with slopes and R² values indicated. The legend presents substances, impactors, and linear regression fits.

4. Conclusion

This study provides a detailed characterization and comparison of the performance of four impactors 120R MOUDI, ultraMOUDI, ELPI, and PENS. To understand the impact of the impactors' design on its ability to collect UFP, we examined their pressure drop, cut-off diameters, steepness of cut-off curve, losses, and particle bounce. Under controlled conditions using three test particle mixtures, we showed that not only the impactor design but also the nature of the particles is a reason for differences in the observed results. This was confirmed when we applied the four impactors to ambient air to examine the mass concentrations of six organic markers in UFP. Summarizing, all four impactors were capable of separating and collecting UFP as they all have a cut-off diameter of about 100 nm. More explicitly, they can be characterized as follows:

- The PENS is compact and lightweight, thus portable and suitable for field or personal exposure studies that require mobility. With a sampling flow rate of 4 L/min a smaller air volume is probed when compared to other impactors. This affects the detection limits, while keeping the pressure drop within the device low (about 260 hPa). Thus, the evaporation and mass-loss of semi-volatile compounds is comparably small. The PENS showed an impact of particle bounce, particularly at higher particle concentrations. We showed that the application of a coating largely reduced the transmission of larger particles in the laboratory tests. However, when markers were apparent in high mass concentrations, we observed a high deviation from the other impactors results in the field comparison. This is likely due to the design of the PENS which has a cyclon for pre-separation and only one stage for impaction of larger particles that could be used for applying a coating. Yet, for the particle-bound BaP and BbF and moderate marker mass concentrations, the PENS compared well with the other impactors.

- The ELPI was simplified for this study. When operated in its original set-up, it has the advantage of a parallel online monitoring of the number size distribution. Here, the ELPI showed a sharp cut-off curve for UFP and effectively no transmission of larger particles. Likely this is due to its design with 13 nozzle and impaction pairs, which can retain larger particles and prevent fragments to cascade through the device. However, this comes with an overall loss in the ultrafine fraction (31±7%) and a pressure drop of 690 hPa. The reduced pressure on the filter substrate can lead evaporative loss of semi-volatile substances during sampling, while non-volatile, particle-bound compounds in UFP (e.g. metals, plastics) can be unaffected by this effect.

- The 120R MOUDI has a rotating design, that should distribute particles evenly across the impaction surface, reducing particle build-up and re-entrainment. Indeed, no transmission of larger particles than about 500 nm was observed in our test and the bounce-effect remained comparably small. However, the cut-off curve was relatively broad as can be seen for example from the dp90, which was with about 180 nm the highest among the four tested impactors. Interestingly, in our tests the sharpness of the cut-off curve for the 120R MOUDI was not impacted by the particle

type. The 120R MOUDI has a pressure drop of 600 hPa. Thus, for semi-volatile substances evaporative losses are likely. For future studies, it would be interesting to determine the long-term efficacy of the rotation in minimizing the bounce effect.

- The ultraMOUDI is a non-rotating and reduced variant of the 120R MOUDI. With a pressure drop of 420 hPa, evaporation loss of semi-volatile compounds is less likely compared to the ELPI and 120R MOUDI. Due to a reduced number of nozzle-impactor pairs, it showed fewer losses in the ultrafine range compared to the ELPI and 120R MOUDI. When compared on the basis of the mass concentrations in ambient UFP, the ultraMOUDI agreed well within the measurement uncertainty for the mostly particle-bound BaP, BbF, and 6PPD, and found slightly higher concentrations for the semi-volatile TA, PA, and Levo. Similar to the PENS, we observed transmission of larger particles due to potential particle bounce, yet showed that this effect was reduced with the application of a coating. The ultraMOUDI is smaller and simpler in the handling than the 120R MOUDI and thus can be integrated in automated, standalone low-volume samplers, for instance.

Our findings indicate that separating and collecting UFP for mass-based chemical analysis is challenging. Numerous factors affect the separation and collection of UFPs, complicating the comparability of studies. The nuanced performance differences among the impactors underscore the need for careful consideration of the intended application and the potential artefacts that may arise during sampling and analysis. Each impactor offers unique advantages and limitations, making it essential to match the impactor to the specific research goals and the properties of the particles being studied. Furthermore, the variability between the impactors' performance for the analysis of the six selected organic markers suggests that factors such as chemical composition, particle morphology, and physical interactions with the impactor significantly influence the results, as well.

Code and data availability

The code and data used in this study are available by request to the corresponding authors.

Competing interests

The authors declare that they have no conflict of interest.

Author contributions

EE: measurements, data analysis, writing, original draft, review, editing

AM, DB: DMS500 measurements, data analysis, writing

NG, JSK, MS, RZ, ACN: funding acquisition, conceptionalization, supervision, writing, review, editing, funding acquisition

805

810

815

820

825

830

835

840

845

References

Abdillah, S. F. I. and Wang, Y. F.: Ambient ultrafine particle (PM0.1): Sources, characteristics, measurements and exposure implications on human health, https://doi.org/10.1016/j.envres.2022.115061, 1 February 2023.

850 Baron, P. A. and Willeke, K.: Aerosol Measurement: Principles, Techniques, and Applications, 3rd ed., 2011.

Bayerisches Landesamt für Statistik: Statistik kommunal - Kreisfreie Stadt Bayreuth - 09 462, 1–30 pp., 2022.

Bein, K. J. and Wexler, A. S.: A high-efficiency, low-bias method for extracting particulate matter from filter and impactor substrates, Atmos Environ, 90, 87–95, 2014.

Berner, A., Luerzer, C. H., Pohl, F., Preining, O., and Wagner, P.: The size distribution of the urban aerosol in Vienna, 855 Sci Total Environ, 13, 245–261, 1979.

Bhattarai, H., Saikawa, E., Wan, X., Zhu, H., Ram, K., Gao, S., Kang, S., Zhang, Q., Zhang, Y., Wu, G., Wang, X., Kawamura, K., Fu, P., and Cong, Z.: Levoglucosan as a tracer of biomass burning: Recent progress and perspectives, https://doi.org/10.1016/j.atmosres.2019.01.004, 15 May 2019.

Boskovic, L., Altman, I. S., Agranovski, I. E., Braddock, R. D., Myojo, T., and Choi, M.: Influence of particle shape on 860 filtration processes, Aerosol Science and Technology, 39, 1184–1190, https://doi.org/10.1080/02786820500442410, 2005.

Brink, J. A.: Cascade Impactor for Adiabatic Measurements, Ind Eng Chem, 50, 645–648, 1958.

Cambustion Ltd.: DMS500 fast particulate analyzer brochure, Cambridge, United Kingdom, 1–6 pp., 2019.

Canepari, S., Astolfi, M. L., Moretti, S., and Curini, R.: Comparison of extracting solutions for elemental fractionation 865 in airborne particulate matter, Talanta, 82, 834–844, https://doi.org/10.1016/j.talanta.2010.05.068, 2010.

Caracci, E., Iannone, A., Carriera, F., Notardonato, I., Pili, S., Murru, A., Avino, P., Campagna, M., Buonanno, G., and Stabile, L.: Size-segregated content of heavy metals and polycyclic aromatic hydrocarbons in airborne particles emitted by indoor sources, Sci Rep, 14, https://doi.org/10.1038/s41598-024-70978-3, 2024.

Chang, M., Kim, S., and Sioutas, C.: Experimental studies on particle impaction and bounce: effects of substrate 870 design and material, Atmospheric Environment, 2313–2322 pp., 1999.

Chen, S. C., Tsai, C. J., Chen, H. D., Huang, C. Y., and Roam, G. D.: The influence of relative humidity on nanoparticle concentration and particle mass distribution measurements by the MOUDI, Aerosol Science and Technology, 45, 596–603, https://doi.org/10.1080/02786826.2010.551557, 2011.

Chen, X., He, T., Yang, X., Gan, Y., Qing, X., Wang, J., and Huang, Y.: Analysis, environmental occurrence, fate and
875   potential toxicity of tire wear compounds 6PPD and 6PPD-quinone, https://doi.org/10.1016/j.jhazmat.2023.131245,
15 June 2023.

Claeys, M., Szmigielski, R., Vermeylen, R., Wang, W., Shalamzari, M. S., and Maenhaut, W.: Tracers for Biogenic
Secondary Organic Aerosol from α-Pinene and Related Monoterpenes: An Overview, https://doi.org/10.1007/978-
94-007-5034-0_18, 2013.

880   Crazzolara, C. and Held, A.: Development of a cascade impactor optimized for size-fractionated analysis of aerosol
metal content by total reflection X-ray fluorescence spectroscopy (TXRF), Atmospheric Measurement Techniques, 17,
2183–2194, 2024.

Daher, N., Ning, Z., Cho, A. K., Shafer, M., Schauer, J. J., and Sioutas, C.: Comparison of the chemical and oxidative
characteristics of particulate matter (PM) collected by different methods: Filters, impactors, and BioSamplers,
885   Aerosol Science and Technology, 45, 1294–1304, https://doi.org/10.1080/02786826.2011.590554, 2011.

Durand, T., Bau, S., Morele, Y., Matera, V., Bémer, D., and Rousset, D.: Quantification of low pressure impactor wall
deposits during ziuc nanoparticle sampling, Aerosol Air Qual Res, 14, 1812–1821,
https://doi.org/10.4209/aaqr.2013.10.0304, 2014.

Fujitani, Y., Hasegawa, S., Fushimi, A., Kondo, Y., Tanabe, K., Kobayashi, S., and Kobayashi, T.: Collection
890   characteristics of low-pressure impactors with various impaction substrate materials, Atmos Environ, 40, 3221–3229,
https://doi.org/10.1016/j.atmosenv.2006.02.001, 2006.

Gong, W.-C., Jidenko, N., Li, Y.-R., Le, T.-C., Borra, J.-P., and Tsai, C.-J.: PM0.1 non-bouncing impactor (NBI) for
ultrafine particle mass and number measurements, J Aerosol Sci, 174, 106249,
https://doi.org/https://doi.org/10.1016/j.jaerosci.2023.106249, 2023.

895   Grieshop, A. P., Donahue, N. M., and Robinson, A. L.: Is the gas-particle partitioning in alpha-pinene secondary
organic aerosol reversible?, Geophys Res Lett, 34, https://doi.org/10.1029/2007GL029987, 2007.

Guo, J., Ji, A., and Xu, Z.: On-site characteristics of airborne particles at a formal electronic waste recycling plant: size
distribution and lung deposited surface area, J Mater Cycles Waste Manag, 25, 346–358,
https://doi.org/10.1007/s10163-022-01536-0, 2023.

900   Hata, M., Linfa, B., Otani, Y., and Furuuchi, M.: Performance evaluation of an Andersen cascade impactor with an
additional stage for nanoparticle sampling, Aerosol Air Qual Res, 12, 1041–1048,
https://doi.org/10.4209/aaqr.2012.08.0204, 2012.

Held, A., Zerrath, A., McKeon, U., Fehrenbach, T., Niessner, R., Plass-Dülmer, C., Kaminski, U., Berresheim, H., and
Pöschl, U.: Aerosol size distributions measured in urban, rural and high-alpine air with an electrical low pressure
905   impactor (ELPI), Atmos Environ, 42, 8502–8512, https://doi.org/10.1016/j.atmosenv.2008.06.015, 2008.

Hillamo, R. E. and Kauppinen, E. I.: On the performance of the berner low pressure impactor, Aerosol Science and Technology, 14, 33–47, https://doi.org/10.1080/02786829108959469, 1991.

Huang, Z., Harrison, R. M., Allen, A. G., James, J. D., Tilling, R. M., and Yin, J.: Field intercomparison of filter pack and impactor sampling for aerosol nitrate, ammonium, and sulphate at coastal and inland sites, Atmos Res, 71, 215–232, 910 https://doi.org/10.1016/j.atmosres.2004.05.002, 2004.

Hussain, K., Hoque, R. R., Balachandran, S., Medhi, S., Idris, M. G., Rahman, M., and Hussain, F. L.: Monitoring and Risk Analysis of PAHs in the Environment, in: Handbook of Environmental Materials Management, Springer International Publishing, 1–35, https://doi.org/10.1007/978-3-319-58538-3_29-2, 2018.

Hu, X., Zhao, H. N., Tian, Z., Peter, K. T., Dodd, M. C., and Kolodziej, E. P.: Transformation Product Formation upon 915 Heterogeneous Ozonation of the Tire Rubber Antioxidant 6PPD (N-(1,3-dimethylbutyl)- N'-phenyl- p-phenylenediamine), Environ Sci Technol Lett, https://doi.org/10.1021/acs.estlett.2c00187, 2022.

Järvinen, A., Aitomaa, M., Rostedt, A., Keskinen, J., and Yli-Ojanperä, J.: Calibration of the new electrical low pressure impactor (ELPI+), J Aerosol Sci, 69, 150–159, https://doi.org/10.1016/j.jaerosci.2013.12.006, 2014.

Junkermann, W. and Hacker, J.: Unprecedented levels of ultrafine particles, major sources, and the hydrological cycle, 920 Sci Rep, 12, https://doi.org/10.1038/s41598-022-11500-5, 2022.

Keskinen, J., Pietarinen, K., and Lehtim, M.: Electrical Low Pressure Impactor, J. Aerosol Sci, 23, 1992.

Kim, B., Lee, J. S., Choi, B.-S., Park, S.-Y., Yoon, J.-H., and Kim, H.: Ultrafine Particle Characteristics in a Rubber Manufacturing Factory, Ann Occup Hyg, 57, 728–739, https://doi.org/10.1093/annhyg/mes102, 2013a.

Kim, K. H., Jahan, S. A., Kabir, E., and Brown, R. J. C.: A review of airborne polycyclic aromatic hydrocarbons (PAHs) 925 and their human health effects, https://doi.org/10.1016/j.envint.2013.07.019, 2013b.

Klöckner, P., Seiwert, B., Wagner, S., and Reemtsma, T.: Organic Markers of Tire and Road Wear Particles in Sediments and Soils: Transformation Products of Major Antiozonants as Promising Candidates, Environ Sci Technol, 55, 11723–11732, https://doi.org/10.1021/acs.est.1c02723, 2021.

Kulkarni, P., Baron, P. A., and Willeke, K.: Aerosol Measurment: Principles, Techniques, and Applications., 3rd ed., 930 2011.

Kumar, P., Morawska, L., Birmili, W., Paasonen, P., Hu, M., Kulmala, M., Harrison, R. M., Norford, L., and Britter, R.: Ultrafine particles in cities, https://doi.org/10.1016/j.envint.2014.01.013, 2014.

Kumar, P., Kalaiarasan, G., Porter, A. E., Pinna, A., Kłosowski, M. M., Demokritou, P., Chung, K. F., Pain, C., Arvind, D. K., Arcucci, R., Adcock, I. M., and Dilliway, C: An overview of methods of fine and ultrafine particle collection for 935 physicochemical characterisation and toxicity assessments, https://doi.org/10.1016/j.scitotenv.2020.143553, 20 February 2021.

Kumsanlas, N., Piriyakarnsakul, S., Sok, P., Hongtieab, S., Ikemori, F., Szymanski, W. W., Hata, M., Otani, Y., and Furuuchi, M.: A cascade air sampler with multi-nozzle inertial filters for PM0.1, Aerosol Air Qual Res, 19, 1666–1677, https://doi.org/10.4209/aaqr.2019.02.0066, 2019.

940   Lai, C. Y., Huang, S. H., Chang, C. P., and Lin, J. Y.: Reducing particle bounce and loading effect for a multi-hole impactor, Aerosol Science and Technology, 42, 114–122, https://doi.org/10.1080/02786820701809045, 2008.

Liu, C.-N., Awasthi, A., Hung, Y.-H., and Tsai, C.-J.: Collection efficiency and interstage loss of nanoparticles in micro-orifice-based cascade impactors, Atmos Environ, 69, 325–333, https://doi.org/https://doi.org/10.1016/j.atmosenv.2012.12.003, 2013.

945   Maharaj Kumari, K. and Lakhani, A.: PAHs in Gas and Particulate Phases: Measurement and Control, in: Environmental Contaminants: Measurement, Modelling and Control, edited by: Gupta, T., Agarwal, A. K., Agarwal, R. A., and Labhsetwar, N. K., Springer Singapore, Singapore, 43–75, https://doi.org/10.1007/978-981-10-7332-8_3, 2018.

Manoli, E., Kouras, A., Karagkiozidou, O., Argyropoulos, G., Voutsa, D., and Samara, C.: Polycyclic aromatic
950   hydrocarbons (PAHs) at traffic and urban background sites of northern Greece: source apportionment of ambient PAH levels and PAH-induced lung cancer risk, Environmental Science and Pollution Research, 23, 3556–3568, https://doi.org/10.1007/s11356-015-5573-5, 2016.

Marjamäki, M., Keskinen, J., Chen, D.-R., and Pui, D. Y. H.: Perfomance Evaluation of the Electrical Low-Pressure Impactor (ELPI), J. Aerosol Sci, 31, 249–261, 2000.

955   Marjamak, M., Keskinen, J., Chen, D.-R., and Pui, D. Y. H.: PERFORMANCE EVALUATION OF THE ELECTRICAL LOW-PRESSURE IMPACTOR (ELPI), J. Aerosol Sci, 249–261 pp., 2000.

Marple, V., Olson, B., Romay, F., Hudak, G., Geerts, S. M., and Lundgren, D.: Second generation micro-orifice uniform deposit impactor, 120 MOUDI-II: Design, Evaluation, and application to long-term ambient sampling, Aerosol Science and Technology, 48, 427–433, https://doi.org/10.1080/02786826.2014.884274, 2014.

960   Marple, V. A. and Willeke, K.: IMPACTOR DESIGN, Pergamon Press, 891–896 pp., 1976.

Marple, V. A., Rubow, K. L., and Behm, S. M.: A microorifice uniform deposit impactor (moudi): Description, calibration, and use, Aerosol Science and Technology, 14, 434–436, https://doi.org/10.1080/02786829108959504, 1991.

Matthew, B. M., Middlebrook, A. M., and Onasch, T. B.: Collection efficiencies in an aerodyne aerosol mass
965   spectrometer as a function of particle phase for laboratory generated aerosols, Aerosol Science and Technology, 42, 884–898, https://doi.org/10.1080/02786820802356797, 2008.

May, K. R.: The Cascade Impactor: An Instrument for Sampling Coarse Aerosols, J. Sci. Instrum, 22, 187–195, 1945.

Mitchell, R. I. and Pilcher, J. M.: Measuring Aerosol Particle Sizes in Air pollutants, Commercial aerosols and Cigarette smoke, Indus. Eng. Chem., 51, 1039–1042, 1959.

970 Mühlbauer, W., Zöllner, C., Lehmann, S., Lorenz, S., and Brüggemann, D.: Correlations between physicochemical properties of emitted diesel particulate matter and its reactivity, Combust Flame, 167, 39–51, https://doi.org/10.1016/j.combustflame.2016.02.029, 2016.

Müller, K., Spindler, G., Van Pinxteren, D., Gnauk, T., Iinuma, Y., Brüggemann, E., and Herrmann, H.: Ultrafine and fine particles in the atmosphere - Sampling, chemical characterization and sources, Chem Ing Tech, 84, 1130–1136,
975 https://doi.org/10.1002/cite.201100208, 2012.

Newton, G. J., Cheng, Y. S., Barr, E. B., and Yeh, H. C.: EFFECTS OF COLLECTION SUBSTRATES ON PERFORMANCE AND WALL LOSSES IN CASCADE IMPACTORS, J. Aerosol Sci, 467–470 pp., 1990.

Ngagine, S. H., Deboudt, K., Flament, P., Choël, M., Kulinski, P., and Marteel, F.: Development and Characterization of a Time-Sequenced Cascade Impactor: Application to Transient PM2.5 Pollution Events in Urbanized and Industrialized
980 Environments, Atmosphere (Basel), 13, https://doi.org/10.3390/atmos13020244, 2022.

Ofner, J., Krüger, H. U., Grothe, H., Schmitt-Kopplin, P., Whitmore, K., and Zetzsch, C.: Physico-chemical characterization of SOA derived from catechol and guaiacol - A model substance for the aromatic fraction of atmospheric HULIS, Atmos Chem Phys, 11, 1–15, https://doi.org/10.5194/acp-11-1-2011, 2011.

Pak, S. S., Liu, B. Y. H., and Rubow, K. L.: Effect of coating thickness on particle bounce in inertial impactors, Aerosol
985 Science and Technology, 16, 141–150, https://doi.org/10.1080/02786829208959544, 1992.

Pomata, D., Di Filippo, P., Riccardi, C., Buiarelli, F., Marini, F., Romani, L., Lucarelli, F., Pazzi, G., Galarini, R., and Simonetti, G.: Concentrations and co-occurrence of 101 emerging and legacy organic pollutants in the ultrafine, fine and coarse fractions of airborne particulates associated with treatment of waste from electrical and electronic equipment, Chemosphere, 338, 139443, https://doi.org/https://doi.org/10.1016/j.chemosphere.2023.139443, 2023.

990 Rao, A. K. and Whitby, K. T.: NON-IDEAL COLLECTION CHARACTERISTICS OF INERTIAL IMPACTORS-I. SINGLE-STAGE IMPACTORS AND SOLID PARTICLES, J, Aerosol Sci, Pergamon Press, 77–86 pp., 1978.

Romay, F. J. and García-Ruiz, E.: Design of Round-Nozzle Inertial Impactors Review with Updated Design Parameters, Aerosol Air Qual Res, 23, https://doi.org/10.4209/aaqr.220436, 2023.

Schwarz, M., Schneider, A., Cyrys, J., Bastian, S., Breitner, S., and Peters, A.: Impact of Ambient Ultrafine Particles on
995 Cause-Specific Mortality in Three German Cities, Am J Respir Crit Care Med, https://doi.org/10.1164/rccm.202209-1837oc, 2023.

Simoneit, B. R. T., Schauer, J. J., Nolte, C. G., Oros, D. R., Elias, V. O., Fraser, M. P., Rogge, W. F., and Cass, G. R.: Levoglucosan, a tracer for cellulose in biomass burning and atmospheric particles, Atmospheric Environment, 173–182 pp., 1999.

1000 de Souza, S. L. Q., Martins, E. M., Corrêa, S. M., da Silva, J. L., de Castro, R. R., and de Souza Assed, F.: Determination of trace elements in the nanometer, ultrafine, fine, and coarse particulate matters in an area affected by light vehicular emissions in the city of Rio de Janeiro, https://doi.org/10.1007/s10661-021-08891-9, 1 February 2021.

Symonds, J., Collings, N., StJReavell, K., and Kittelson, D.: Evaporation of Volatile Aerosols, ETH Hönggerberg, 2004.

1005 Symonds, J. P. R., Reavell, K. S. J., Olfert, J. S., Campbell, B. W., and Swift, S. J.: Diesel soot mass calculation in real-time with a differential mobility spectrometer, J Aerosol Sci, 38, 52–68, https://doi.org/10.1016/j.jaerosci.2006.10.001, 2007.

Thongyen, T., Hata, M., Toriba, A., Ikeda, T., Koyama, H., Otani, Y., and Furuuchi, M.: Development of PM0.1 personal sampler for evaluation of personal exposure to aerosol nanoparticles, Aerosol Air Qual Res, 15, 180–187, https://doi.org/10.4209/aaqr.2014.05.0102, 2015.

1010 Tsai, C. J., Liu, C. N., Hung, S. M., Chen, S. C., Uang, S. N., Cheng, Y. S., and Zhou, Y.: Novel active personal nanoparticle sampler for the exposure assessment of nanoparticles in workplaces, Environ Sci Technol, 46, 4546–4552, https://doi.org/10.1021/es204580f, 2012.

Turner, J. R. and Hering, S. V: GREASED AND OILED SUBSTRATES AS BOUNCE-FREE IMPACTION SURFACES, J. Aerosol Sci, 215–224 pp., 1987.

1015 Ungeheuer, F., Van Pinxteren, D., and Vogel, A. L.: Identification and source attribution of organic compounds in ultrafine particles near Frankfurt International Airport, Atmos Chem Phys, 21, 3763–3775, https://doi.org/10.5194/acp-21-3763-2021, 2021.

Vestenius, M., Hellén, H., Levula, J., Kuronen, P., Helminen, K. J., Nieminen, T., Kulmala, M., and Hakola, H.: Acidic reaction products of monoterpenes and sesquiterpenes in atmospheric fine particles in a boreal forest, Atmos Chem
1020 Phys, 14, 7883–7893, https://doi.org/10.5194/acp-14-7883-2014, 2014.

Wang, G., Huang, L., Xin Zhao, Niu, H., and Dai, Z.: Aliphatic and polycyclic aromatic hydrocarbons of atmospheric aerosols in five locations of Nanjing urban area, China, Atmos Res, 81, 54–66, https://doi.org/10.1016/j.atmosres.2005.11.004, 2006.

Wiedensohler, A., Birmili, W., Nowak, A., Sonntag, A., Weinhold, K., Merkel, M., Wehner, B., Tuch, T., Pfeifer, S.,
1025 Fiebig, M., Fjäraa, A. M., Asmi, E., Sellegri, K., Depuy, R., Venzac, H., Villani, P., Laj, P., Aalto, P., Ogren, J. A., Swietlicki, E., Williams, P., Roldin, P., Quincey, P., Hüglin, C., Fierz-Schmidhauser, R., Gysel, M., Weingartner, E., Riccobono, F., Santos, S., Grüning, C., Faloon, K., Beddows, D., Harrison, R., Monahan, C., Jennings, S. G., O'Dowd, C. D., Marinoni, A., Horn, H. G., Keck, L., Jiang, J., Scheckman, J., McMurry, P. H., Deng, Z., Zhao, C. S., Moerman, M., Henzing, B., De Leeuw, G., Löschau, G., and Bastian, S.: Mobility particle size spectrometers: Harmonization of technical standards
1030 and data structure to facilitate high quality long-term observations of atmospheric particle number size distributions, Atmos Meas Tech, 5, 657–685, https://doi.org/10.5194/amt-5-657-2012, 2012.

Wiedensohler, A., Wiesner, A., Weinhold, K., Birmili, W., Hermann, M., Merkel, M., Müller, T., Pfeifer, S., Schmidt, A., Tuch, T., Velarde, F., Quincey, P., Seeger, S., and Nowak, A.: Mobility particle size spectrometers: Calibration procedures and measurement uncertainties, Aerosol Science and Technology, 52, 146–164,
1035 https://doi.org/10.1080/02786826.2017.1387229, 2018.

Won Kim, S.: Critical Review on Evaporative Loss of Semivolatile Aerosols during Sampling, J. Env. Hlth. Sci, 171–181 pp., 2010.

Xie, M., Hannigan, M. P., and Barsanti, K. C.: Gas/particle partitioning of 2-methyltetrols and levoglucosan at an urban site in Denver, Environ Sci Technol, 48, 2835–2842, https://doi.org/10.1021/es405356n, 2014.

1040 Yao, Y., Ye, X., Gao, T., Feng, H., Chen, Y., and Chen, J.: Significant impactor sampling artifacts of ammonium, nitrate, and organic acids, Atmos Environ, 274, https://doi.org/10.1016/j.atmosenv.2022.118985, 2022.

Young, L. H., Lin, Y. H., Lin, T. H., Tsai, P. J., Wang, Y. F., Hung, S. M., Tsai, C. J., and Chen, C. W.: Field application of a newly developed personal nanoparticle sampler to selected metalworking operations, Aerosol Air Qual Res, 13, 849–861, https://doi.org/10.4209/aaqr.2012.10.0270, 2013a.

1045 Young, L. H., Lin, Y. H., Lin, T. H., Tsai, P. J., Wang, Y. F., Hung, S. M., Tsai, C. J., and Chen, C. W.: Field application of a newly developed personal nanoparticle sampler to selected metalworking operations, Aerosol Air Qual Res, 13, 849–861, https://doi.org/10.4209/aaqr.2012.10.0270, 2013b.

Zhao, Z., Hao, J., LI, J., and WU, S.: Second organic aerosol formation from the ozonolysis of α-pinene in the presence of dry submicron ammonium sulfate aerosol, Journal of Environmental Sciences, 20, 1183–1188,
1050 https://doi.org/10.1016/S1001-0742(08)62207-X, 2008.

Zhu, C.-S., Cao, J.-J., Tsai, C.-J., Zhang, Z.-S., and Tao, J.: Biomass burning tracers in rural and urban ultrafine particles in Xi'an, China, Atmos Pollut Res, 8, 614–618, https://doi.org/https://doi.org/10.1016/j.apr.2016.12.011, 2017.

1055

1060

1065

1070

1075